Applied Catalysis B: Environmental 197 (2016) 168–183

Contents lists available at ScienceDirect

Applied Catalysis B: Environmental

journal homepage: www.elsevier.com/locate/apcatb

Dry reforming of methane over 5 wt% Ni/$Ce_{1-x}Pr_xO_{2-\delta}$ catalysts: Performance and characterisation of active and inactive carbon by transient isotopic techniques

M.A. Vasiliades[a], M.M. Makri[a], P. Djinović[b], B. Erjavec[b], A. Pintar[b], A.M. Efstathiou[a,*]

[a] Department of Chemistry, Heterogeneous Catalysis Laboratory, University of Cyprus, 1 University Ave., University Campus, P.O. Box 20537, CY 1678 Nicosia, Cyprus
[b] Laboratory for Environmental Sciences and Engineering, National Institute of Chemistry, Hajdrihova 19, SI-1001 Ljubljana, Slovenia

ARTICLE INFO

Article history:
Received 19 December 2015
Received in revised form 20 February 2016
Accepted 5 March 2016
Available online 8 March 2016

Keywords:
Dry reforming of methane
Transient carbon oxidation (TPO)
SSITKA
DRM mechanism
Ceria-praseodymia supported Ni

ABSTRACT

The effects of $Ce_{1-x}Pr_xO_{2-\delta}$ support composition (x = 0.0–0.8) and reaction temperature (550–750 °C) on the catalytic activity and selectivity and important features of the mechanism of the dry reforming of methane (DRM) over supported Ni (5 wt%) were investigated. Of particular interest were the effects on the concentration of *active* and *inactive* carbon formed, the relative contribution of CH_4 and CO_2 activation routes towards carbon formation and the structure and morphology of the inactive carbon which was formed. For these carbon characterization studies, steady-state isotopic transient kinetic analysis ($^{13}CO_2$-SSITKA), temperature-programmed oxidation (TPO) following $^{13}CO_2/^{12}CH_4$/He dry reforming, thermal gravimetric analysis coupled with TPO (TGA-TPO), scanning electron miscroscopy (SEM-EDX) and transmission electron microscopy with atomic resolution (HRTEM) and powder X-ray diffraction (XRD) were employed. The relative amount of *inactive* carbon formed via the CH_4 and CO_2 activation routes was found to strongly depend on reaction temperature and Pr-dopant support composition. At 550 °C, the contribution of the CO_2 activation route to the *inactive* carbon formation (besides that of the CH_4 activation route) was 65.7 and 60.1%, respectively, for Ni supported on CeO_2 and $Ce_{0.2}Pr_{0.8}O_2$ carriers, whereas at 750 °C the respective values were 54.0 and 50.9%. Filamentous carbon and thin layers of graphitic carbon were identified as the main morphologies of *inactive* carbon. The surface coverage of *active* carbon that truly participates in the formation of CO was found to depend on support composition and reaction temperature (θ_C = 0.03–0.15 at 550 °C and 0.07–3.4 at 750 °C). A pool of *inactive* reversibly adsorbed CO_2 was measured (θ = 1.5–4.1) for the first time, which was dependent on support composition and reaction T. The introduction of 20 atom-% Pr in the ceria lattice caused a significant reduction in the rate of *inactive* carbon formation with marginal decrease in catalyst's activity and stability after 25 h on stream. Further introduction of Pr-dopant (80 atom-%) caused drastic reduction in the deposited carbon after 25 h on the reaction stream at 750 °C (0.07 wt% C) but with appreciable decrease in CH_4- and CO_2-conversions and H_2/CO gas-product ratio (a drop by a factor of 1.85, 1.45 and 1.47, respectively). The latter decrease in catalyst's performance is correlated with the increase in the pool of inactive adsorbed CO_2 in the form of carbonate-like species.

1. Introduction

Dry reforming of methane, DRM ($CH_4 + CO_2 \leftrightarrow 2CO + 2H_2$, $\Delta H^\circ = +261$ kJ mol^{-1}) technology has been investigated intensively and has drawn industrial attention since it offers advantages of converting CH_4 and CO_2 into liquid fuels and other chemicals (favourable H_2/CO ratio) compared to the classical steam methane reforming technology [1–7]. In addition, DRM could result in lower operating cost amongst the currently operating methane reforming processes: steam reforming, partial oxidation and autothermal reforming, under certain conditions [8]. Dry reforming of methane also offers valuable environmental benefits, such as biogas utilisation, removal of GHG (methane and carbon dioxide) and conversion of natural gas with a high CO_2 content into valuable syngas [1].

Dry reforming of methane despite having all the above mentioned benefits and advantages has not yet found an industrial

* Corresponding author.
E-mail address: efstath@ucy.ac.cy (A.M. Efstathiou).

http://dx.doi.org/10.1016/j.apcatb.2016.03.012
0926-3373/

development since the so far developed low-cost Ni-based catalysts suffer from deactivation due to "carbon" deposition [1–7]. The formation of "carbon" originates from methane decomposition (Eq. (1)) and the Boudouard reaction (Eq. (2)) [2,5]:

$$CH_4 \rightarrow C\text{-}s + 2H_2,\ \Delta H^\circ = +75\ kJ\ mol^{-1} \quad (1)$$

$$2CO \leftrightarrow C\text{-}s + CO_2,\ \Delta H^\circ = -172\ kJ\ mol^{-1} \quad (2)$$

It should be noted that part of the surface carbon appearing in Eqs. (1)–(2) comprises the *active* carbon pool that eventually forms CO(g), whereas the rest of it comprises the *inactive* "carbon": graphite whiskers, carbon fibres and amorphous carbon [1,6].

Much research effort has been recently devoted towards the design of suitable supported Ni-based catalysts for the dry reforming of methane with significant suppression in "carbon" deposition, thus improving catalyst's durability. Important catalyst design parameters include support chemical composition and the use of chemical promoters [1–7]. One of the approaches in finding suitable supports for nickel is the utilisation of metal oxides possessing high oxygen storage capacity (OSC), which proved to increase "carbon" formation resistance but also to mitigate sintering of metallic nickel [2,9]. In particular, ceria-zirconia solid solutions have been reported to exhibit significant improvements in "carbon" formation reduction and catalyst's stability compared to other non-reducible metal oxides (e.g. γ-Al_2O_3, SiO_2) used as carriers of nickel [2,10–21].

An in-depth investigation of the oxygen vacancy effect in other than Zr^{4+}-doped CeO_2 supports for nickel in the DRM reaction appears to be limited. In particular, praseodymium (Pr), one of the multivalent elements used for dissolution into the ceria matrix, shows excellent OSC behaviour [22–24], DRM activity and stability [10,25]. Recently, $Ce_{0.9}Pr_{0.1}O_2$-supported Ir catalysts have been reported to be highly efficient DRM catalysts after tuning the Ir-support interactions by adopting different preparation techniques [26].

In spite of efforts to develop suitable CeO_2-doped supported Ni catalysts towards sustainable DRM activity, fundamental understanding of the relative importance of each of the "carbon" formation chemical routes (Eqs. (1)–(2)) over these catalysts has only recently been reported [25] for 5 wt% $Ni/Ce_{1-x}M_xO_{2-\delta}$ (M = Zr, Pr) and previously for Ni/SiO_2 [27], Ni/Al_2O_3—CaO [28] and Ni/La_2O_3 [29] catalytic systems after using $^{13}CH_4$ or $^{13}CO_2$ isotope gas coupled with temperature-programmed oxidation (TPO) and other transient experiments.

The present work addresses the catalytic performance of $Ce_{1-x}Pr_xO_{2-\delta}$-supported Ni (5 wt%) in the dry reforming of CH_4 (550–750 °C), where for the first time the effects of Pr/Ce atom ratio on (i) the concentration of *active* "carbon" formed via the CO_2 activation route, (ii) the concentration and structure/morphology of *inactive* carbon and its reactivity towards oxygen, (iii) the relative contribution of the CH_4 and CO_2 activation routes to the total "carbon" formation and (iv) the TOF_{ITK} (s^{-1}) based on the mean life-time of *active* intermediates are reported. For this purpose, steady-state isotopic transient kinetic analysis (SSITKA), temperature-programmed oxidation (TPO) after DRM (use of $^{12}CO_2$ or $^{13}CO_2$), powder XRD, HRTEM-EDXS, SEM and TGA-TPO techniques were employed.

2. Experimental

2.1. Catalyst preparation

The $Ce_{1-x}Pr_xO_{2-\delta}$ (x = 0.0, 0.2, 0.5, 0.65 and 0.8) solid supports were synthesized using the citrate sol-gel method [30–32]. The metal precursors used were $Ce(NO_3)_3{\cdot}6H_2O$ and $Pr(NO_3)_3{\cdot}6H_2O$ (Sigma-Aldrich). The resulting material was dried at 120 °C for 17 h. Heating of the material in a furnace (ELF 11/6, Carbolite) from room T to 400 °C in static air (2 °C/min) was then applied, where self-ignition took place at ~350 °C. The material was kept at 400 °C for 30 min. The sample was then left to cool to room T and after being grinded, the resulting solid was calcined at 500 °C for 6 h (static air, 2 °C/min from room T to 500 °C), and then at 750 °C for an additional 4 h. The $Ni/Ce_{1-x}Pr_xO_{2-\delta}$ catalysts were prepared by impregnating the supports with a given amount of diluted aqueous solution of $Ni(NO_3)_2{\cdot}6H_2O$ (Sigma-Aldrich) so as to yield a 5 wt% Ni nominal loading. The resulting slurry was dried overnight and then calcined (static air) at 750 °C for 4 h. The catalyst sample thus obtained (named fresh) before any catalytic measurements (activity and characterisation of "carbon") was *in situ* reduced in H_2 flow (1 bar, 50 NmL min^{-1}) at 700 °C for 2 h.

2.2. Catalyst characterization

2.2.1. Powder X-ray diffraction

The $Ce_{1-x}Pr_xO_{2-\delta}$-supported Ni fresh catalysts were recalcined at 650 °C for 1 h before transferred to a Shimadzu 6000 Series diffractometer (CuKa radiation, λ = 1.5418 Å) for powder XRD analyses. Powder X-ray diffractograms were recorded in the 20–80° 2θ range (scan speed = 2°/min). The lattice parameter (α, Å) and the mean volume primary crystallite size (d_c, nm) of support's single-phase solid solution and that of NiO phase were estimated as recently reported [25]. The 5 wt% Ni/CeO_2 catalyst that presented the largest amount of "carbon" deposits after 25 h of dry reforming at 750 °C was also checked for alterations in the d_c (nm) of both the nickel and support crystal phases but also for the formation of graphitic carbon.

2.2.2. Specific surface area and pore size distribution

The specific surface area (SSA, $m^2\ g^{-1}$) and the mean pore size (d_p, nm) of the $Ce_{1-x}Pr_xO_{2-\delta}$ solids were determined by N_2 adsorption-desorption isotherms at liquid N_2 temperature (77 K, BET method) using a Micromeritics® Gemini surface area and pore size analyser. Before measurements, the samples were *in situ* degassed at 300 °C for 3 h in pure N_2 gas flow to remove adsorbed atmospheric water and most of the CO_2.

2.2.3. H_2 temperature-programmed desorption (TPD) studies

Prior to the H_2-TPD run, the fresh catalyst sample (0.5 g) was first reduced in H_2 gas flow (1 bar) at 700 °C for 2 h. The catalyst was then purged in He flow to 750 °C to remove hydrogen that might have been spilled over the support (until hydrogen signal in the mass spectrometer reached the background value in He), and then cooled in He flow to 25 °C. Hydrogen chemisorption was performed using a diluted 0.3 vol% H_2/He gas mixture for 30 min at 25 °C in order to minimize hydrogen spillover. Following this adsorption step, the catalyst and gas lines were purged in He flow for 10 min. The catalyst was then heated to 750 °C in He flow (50 NmL/min, β=30 °C/min) for the TPD run. The H_2 signal (m/z = 2) was continuously monitored with *on line* mass spectrometer, MS (Balzers, Omnistar 1–200 amu) and converted into concentration (mol%) using a standard 0.1 vol% H_2/He gas mixture. Nickel dispersion (D, %) was estimated after considering an H/Ni_s = 1. The Ni mean primary particle size, d_{Ni} (nm) was estimated using the following Eq. (3) [33]:

$$< d_{Ni} > (nm) = 0.97/D(\%) \times 100 \quad (3)$$

2.2.4. Morphology of $Ni/Ce_{1-x}Pr_xO_{2-\delta}$ catalysts

The morphology of the fresh and spent $Ce_{1-x}Pr_xO_{2-\delta}$-supported Ni catalysts was characterized by means of scanning electron microscopy (SEM) (Carl Zeiss, model FE-SEM SUPRA 35VP). Transmission electron microscope (TEM) with atomic resolution (JEOL ARM 200CF) equipped with a cold field-emission gun, probe spheri-

cal aberration corrector (CESCOR unit from CEOS) and Jeol Centurio EDXS system with 100 mm^2 SDD detector was used to examine details of the morphology of selected catalyst samples.

2.3. Catalytic performance of $Ni/Ce_{1-x}Pr_xO_{2-\delta}$ solids

The experimental apparatus used for evaluating the catalytic performance of the 5 wt% $Ni/Ce_{1-x}Pr_xO_{2-\delta}$ solids was previously described [34]. Prior to any catalytic measurements, the fresh solid was reduced in H_2 (1 bar, 50 NmL min^{-1}) at 700 °C for 2 h. The reaction feed consisted of 20 vol% CO_2/20 vol% CH_4/60 vol% He, the total volume flow rate was 150 NmL min^{-1}, and the catalytic bed consisted of 0.15 g of catalyst (W_{cat}) and 0.15 g of SiC (to minimize heat transfer effects within the catalytic bed) homogeneously mixed (particle size 0.1–0.3 mm), resulting in a GHSV of ~30,000 h^{-1} ($L/L_{catbed}/h$). The outlet feed gas stream from the reactor was directed to a mass spectrometer (Omnistar 1–300 amu, Balzer) for on line monitoring of CH_4 (m/z = 15), H_2 (m/z = 2) and C_2H_6 (m/z = 30) and to an infrared gas analyzer (Horiba, model VA-3000) for CO and CO_2. The catalytic performance of the $Ni/Ce_{1-x}Pr_xO_{2-\delta}$ solids was evaluated in the 550–750 °C range based on the CO_2 (X_{CO2}, %) and CH_4 (X_{CH4}, %) conversion relationships previously reported [25]. Calibration of the MS and infrared CO/CO_2 analyzer signals to concentration (mol%) was performed using standard calibration gas mixtures diluted in He gas. The H_2 and CO product yields (%) were estimated using the following Eq. (4) and Eq. (5), respectively:

$$Y_{H_2}(\%) = \frac{F_{H_2}^{out}}{2F_{CH_4}^{in}} \times 100 \quad (4)$$

$$Y_{CO}(\%) = \frac{F_{CO}^{out}}{F_{CH_4}^{in} + F_{CO_2}^{in}} \times 100 \quad (5)$$

where $F_{CH_4}^{in}$ and $F_{CO_2}^{in}$ are the molar flow rates (mols s^{-1}) of CH_4 and CO_2, respectively, at the reactor inlet, whereas $F_{H_2}^{out}$ and F_{CO}^{out} are the molar flow rates (mols s^{-1}) of H_2 and CO at the reactor outlet, respectively. Catalytic measurements were obtained after 30 min on reaction stream in the 550–750 °C range starting from the lowest T of 550 °C. At the end of the 30-min dry reforming, the catalyst was exposed to 20 vol% H_2/He gas flow and the temperature was increased to 750 °C until no methane was recorded in the MS before cooled in He flow to the next reaction temperature. A catalytic experiment using 0.15 g of pure SiC revealed no activity at the dry reforming conditions applied. The stability performance of all 5 wt% $Ni/Ce_{1-x}Pr_xO_{2-\delta}$ catalysts was recorded at 750 °C for a period of 25 h on reaction stream.

2.4. Characterization of deposited "carbon" by transient methods

2.4.1. Temperature-programmed oxidation (TPO)

The reactivity towards oxygen and the amount (μmol g^{-1} or mg g^{-1}) of the "carbon" formed after 25 h of dry reforming at 750 °C were investigated by TPO. After DRM the feed was changed to He for 20 min at 750 °C, where at the end of the He purge the CO_2, CO, H_2 and CH_4 signals in the MS reached their respective background value. The catalyst (0.15 g + 0.15 g SiC) temperature was then increased to 800 °C in He gas flow and kept at this temperature until no CO or CO_2 signal was recorded in the MS. The catalyst was then cooled in He flow to 100 °C and the feed was switched to 10 vol% O_2/He (50 N mL min^{-1}), while the temperature of the catalyst had increased to 800 °C (TPO run, 30 °C min^{-1}). The CO (m/z = 28) and CO_2 (m/z = 44) signals in the MS were continuously monitored and their quantification was made using certified calibration gas mixtures (ca. 2 mol% CO/He and 945 ppm CO_2/He).

2.4.2. TGA-Temperature-programmed oxidation (TPO) –CHNS

The amount of "carbon" accumulated on the surface of 5 wt% $Ni/Ce_{1-x}Pr_xO_{2-\delta}$ catalysts after 25 h of dry reforming at 750 °C while using 0.3 g of catalyst (no SiC, same reactor as that used in TPO experiments) was also determined by means of CHNS elemental (PerkinElmer, model 2400 Series II) and thermogravimetric analysis (TGA) (Perkin Elmer, model STA 6000). Prior to TGA the samples were dried *in situ* in air flow (50 N mL/min) at 80 °C for 30 min. Subsequently, the sample temperature was increased maintaining the same gas flow rate to 900 °C with a heating rate of 10 °C min^{-1}.

2.5. Contribution of CO_2 and CH_4 activation routes to the formation of "carbon"

Temperature-programmed oxidation (TPO) following dry reforming and having labelled the carbon dioxide in the feed stream (use of $^{13}CO_2$) has been conducted in order to estimate the relative contribution of the CO_2 and CH_4 activation routes towards the formation of "carbon" deposits. The experimental procedure was as follows. After reforming at 550 or 750 °C for 30 min (5 vol% $^{13}CO_2$/5 vol% $^{12}CH_4$/45 vol% Ar/45 vol% He; 100 NmL/min; W_{cat} = 0.2 g), the reactor was purged in He flow for 10 min and the temperature was then increased to 750 °C (DRM performed at 550 °C) and kept at this temperature until background values were reached for the CO and CO_2 MS signals. The catalyst sample was then cooled in He flow to 200 °C and the feed was switched to a 10 vol% O_2/He (50 NmL min^{-1}) gas mixture while simultaneously increasing the temperature to 750 °C (β = 30 °C/min, TPO run). The mass numbers (m/z) 45 ($^{13}CO_2$), 44 ($^{12}CO_2$), 29 (^{13}CO) and 28 (^{12}CO) in the MS were continuously monitored. The amount (μmol g^{-1}) of "carbon" derived from the CO_2 activation route was estimated after integrating the ^{13}CO and $^{13}CO_2$ TPO traces, while that derived from the $^{12}CH_4$ activation route after integrating the ^{12}CO and $^{12}CO_2$ TPO traces.

2.6. SSITKA studies – tracing the CO_2 activation route

Steady-state isotopic transient kinetic analysis (SSITKA) experiments using $^{13}CO_2$ in the feed stream (5 vol% $^{13}CO_2$/5 vol% $^{12}CH_4$/45 vol% Ar/45 vol% He; 100 NmL/min) were operated at low CH_4 conversions at 550 °C (lower than 15%, W_{cat} = 0.1 g) and at high CH_4 conversions at 750 °C (integral reaction conditions, W_{cat} = 0.03 g) in order to accurately trace the *carbon path* of the CO_2 activation route. The following SSITKA switches were performed: $^{12}CO_2/^{12}CH_4$/Ar/He (T, 2 h) → $^{13}CO_2/^{12}CH_4$/Kr/Ar/He (T, 20 min) → $^{12}CO_2/^{12}CH_4$/Ar/He (T, t). At the last switch, the decay of Kr, ^{13}CO and $^{13}CO_2$ signals were continuously monitored by on line MS from which the amount of *active carbon-containing* reaction intermediates was estimated after using the following relationship:

$$N_c(molC/g_{cat}) = (F_T y_{13CO}(s.s.)/W_{cat}) \int_{t=0}^{t^f} [Z_{13CO}(t) - Z_{13CO2}(t)]dt \quad (6)$$

where F_T is the total molar flow rate (mols s^{-1}) of the $^{13}CO_2/^{12}CH_4$/Kr/Ar/He feed, y_{13CO} (s.s.) is the steady-state mole fraction of ^{13}CO(g) formed in the reaction product gas stream after 20 min of reaction (new steady-state) and Z_{13CO} and Z_{13CO2} are the dimensionless concentrations of gaseous ^{13}CO and $^{13}CO_2$ [35,36]. t = 0 is the time the Kr signal at the switch $^{13}CO_2/^{12}CH_4$/Kr/Ar/He → $^{12}CO_2/^{12}CH_4$/Ar/He starts to decay, whereas t^f is the final time at which the new steady-state under the non isotopic feed is obtained.

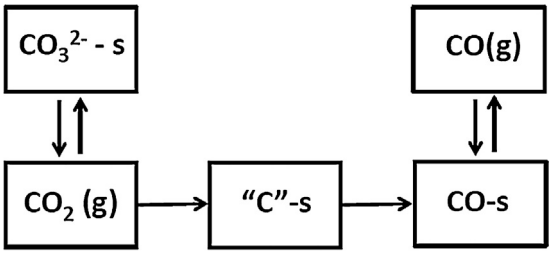

Scheme 1. The SSITKA formalism for the activation path of CO_2 towards the formation of CO in the DRM reaction over 5 wt% Ni/$Ce_{1-x}Pr_xO_{2-\delta}$ catalysts. "C"-s is the pool of active carbon species, CO-s is the pool of adsorbed CO, and CO_3^{2-}-s is the pool of non-active reversibly formed carbonate-type species on the $Ce_{1-x}Pr_xO_{2-\delta}$ support.

According to the SSITKA theory and its interconnected pools formalism depicted in Scheme 1, N_C represents the sum of the concentrations of "C"-s and CO-s active reaction intermediates. The nature of "C"-s will be discussed below. It is possible to estimate the amount (mol g_{cat}^{-1}) of *reversibly adsorbed* CO_2 formed on the catalyst surface (e.g. CO_2 – s1 and/or CO_3^{2-} – s2) under dry reforming, which is considered as spectator (*inactive*) species after using the following relationship:

$$N_{CO2}(mol/g_{cat}) = \left([F_T y^f_{13CO2}(1 - X_{13CO2})] / W_{cat} \right) \int_{t=0}^{t^f} [Z_{13CO2}(t) - Z_{Kr}(t)]dt \quad (7)$$

where y^f_{13CO2} and X_{13CO2} are the mole fraction of $^{13}CO_2$ in the isotopic feed gas stream and the steady-state $^{13}CO_2$ conversion, respectively. Z_{Kr} is the dimensionless concentration of Kr tracer gas [35,36]; s_1 and s_2 represent catalytic sites on the nickel and metal oxide support surfaces, respectively. The pool of this reversibly adsorbed CO_2 is also depicted in Scheme 1.

The average residence time of the *active* carbon-containing species (C-pool) present in the CO_2 activation path to form CO, τ_C (s), is calculated as the area between the normalized transient response curve of ^{13}CO(g) and that of $^{13}CO_2$(g) in the down-step SSITKA switch $^{13}CO_2/^{12}CH_4$/Ar/Kr/He → $^{12}CO_2/^{12}CH_4$/Ar/He after using the following relationship:

$$\tau_c(s) = \int_{t=0}^{t^f} [Z_{13CO}(t) - Z_{13CO2}(t)]\, dt \quad (8)$$

Based on the SSITKA theory and its formalism [36], the specific kinetic rate of reaction (mol g_{cat}^{-1} s^{-1}) at steady-state is related to the TOF_{ITK} (s^{-1}) by the following relationship:

$$\text{Rate}(\mu\text{mol}\, g^{-1}\, s^{-1}) = TOF_{ITK}\, N_C = N_C(1/\tau_C) \quad (9)$$

where N_C is the concentration (μmol g^{-1}) of *active* reaction intermediates found in the carbon-path probed and which is estimated according to Eq. (6).

3. Results

3.1. Surface texture and powder XRD studies

The specific surface area (SSA), pore volume (V_p) and the mean pore diameter (d_p) for the solid supports investigated are given in Table S1 (Supplementary information). The SSA of the materials is in the 5–12 m^2 g^{-1} range with CeO_2 exhibiting the largest value (12 m^2 g^{-1}). As Pr-dopant is introduced into the CeO_2 lattice, the SSA slightly drops and only after a high loading of Pr-dopant (80 atom-%) is used the SSA drops by a factor of 2.4. The mean pore diameter and pore volume were found to be in the 9–22 nm and 0.033–0.072 cm^3 g^{-1} range, respectively. The d_p shows an increase in the 20–65 atom-% Pr composition range, whereas further increase to 80 atom-% provides no additional change. X-ray diffractograms of fresh 5 wt% Ni/$Ce_{1-x}Pr_xO_{2-\delta}$ solids are given in Fig. S1 (Supplementary information). The $Ce_{1-x}Pr_xO_{2-\delta}$ solids are single-phase homogeneous solid solutions of fluorite cubic structure for the entire Ce-Pr composition range investigated. This is in agreement with TEM/EDXS studies reported below. This result is in excellent agreement with the work of Somacescu et al. [37] for a series of $Ce_{1-x}Pr_xO_{2-\delta}$ solids (x = 0.0, 0.1, 0.5, 0.9) prepared by the self-assembly method assisted by surfactants and hydrothermal treatment and with the work of Ahn et al. [22] who investigated the role of Pr in the formation and migration of oxygen vacancies in Pr-doped ceria ($Ce_{1-x}Pr_xO_2$; x = 0.0–0.5) prepared by the glycine nitrate process. A similar slight shift of 2θ to lower values with increasing Pr content was noticed (Fig. S1) due to the larger ionic radius of Pr^{3+} (1.226 Å), in relation to the Ce^{4+} cation (0.97 Å) [22].

The primary crystallite size of NiO (d_{NiO}, nm) and that of $Ce_{1-x}Pr_xO_{2-\delta}$ support (d_c, nm) were estimated (Table S1). All catalysts exhibit similar NiO particle sizes (~30–35 nm) and support primary crystal size (29–35 nm). Further details and discussion about the XRD results obtained are provided in Supplementary Information.

3.2. TEM-EDXS studies

Fig. 1a and b shows TEM micrographs of fresh 5 wt% Ni/CeO_2 and 5 wt% Ni/$Ce_{0.2}Pr_{0.8}O_{2-\delta}$ catalysts, respectively. Both catalyst supports are comprised of polydisperse agglomerated polyhedral primary crystallites in the 30–50 nm in size range. This size corresponds closely to that of CeO_2 and $Ce_{0.2}Pr_{0.8}O_{2-\delta}$ crystallites estimated from powder XRD (Table S1). EDXS elemental mapping of Ce and Pr in both Ni/$Ce_{0.5}Pr_{0.5}O_{2-\delta}$ and Ni/$Ce_{0.2}Pr_{0.8}O_{2-\delta}$ catalysts shows a very homogeneous distribution of these elements, suggesting the formation of a single-phase homogeneous solid solution, which is in very good agreement with the powder XRD results (Fig. S1). It is noted that the presence of ultra-high vacuum and electron beam flux likely caused reduction of NiO to Ni during TEM-EDX analysis. EDXS mapping analysis revealed that Ni particles in the 5 wt% Ni/CeO_2 range between 30 and 100 nm in size and resemble cubooctahedra in shape. Very similar Ni particle size and shape were also seen in the 5 wt% Ni/$Ce_{0.5}Pr_{0.5}O_{2-\delta}$ and 5 wt% Ni/$Ce_{0.2}Pr_{0.8}O_{2-\delta}$ solids (Supplementary information, Figs. S2–S3 and S4–S6, respectively). TEM and SAED analyses revealed that Ni cubooctahedra (metallic Ni crystallized in cubic Fm3 m space group) predominantly expose group [100] and [111] terminating crystal planes. Some of the Ni particles were confirmed as polysynthetic twin crystals, sharing the [111] twin plane which acts as a boundary between the individual Ni crystallites (Fig. S7). As a result, the visualized Ni particles comprise of smaller primary crystallites in agreement with their size estimation based on the powder XRD and H_2 chemisorption studies. The clear formation of "carbon" layers in several areas of the Ni particle's surface in the spent catalyst should be noted (Fig. S7b, Supplementary information).

3.3. H_2 temperature-programmed desorption (TPD) studies

Fig. 2 presents H_2-TPD traces obtained over 5 wt% Ni supported on CeO_2 (Fig. 2a), $Ce_{0.5}Pr_{0.5}O_{2-\delta}$ (Fig. 2b) and $Ce_{0.2}Pr_{0.8}O_{2-\delta}$ (Fig. 2c) carriers. The total amount of hydrogen desorbed and the asso-

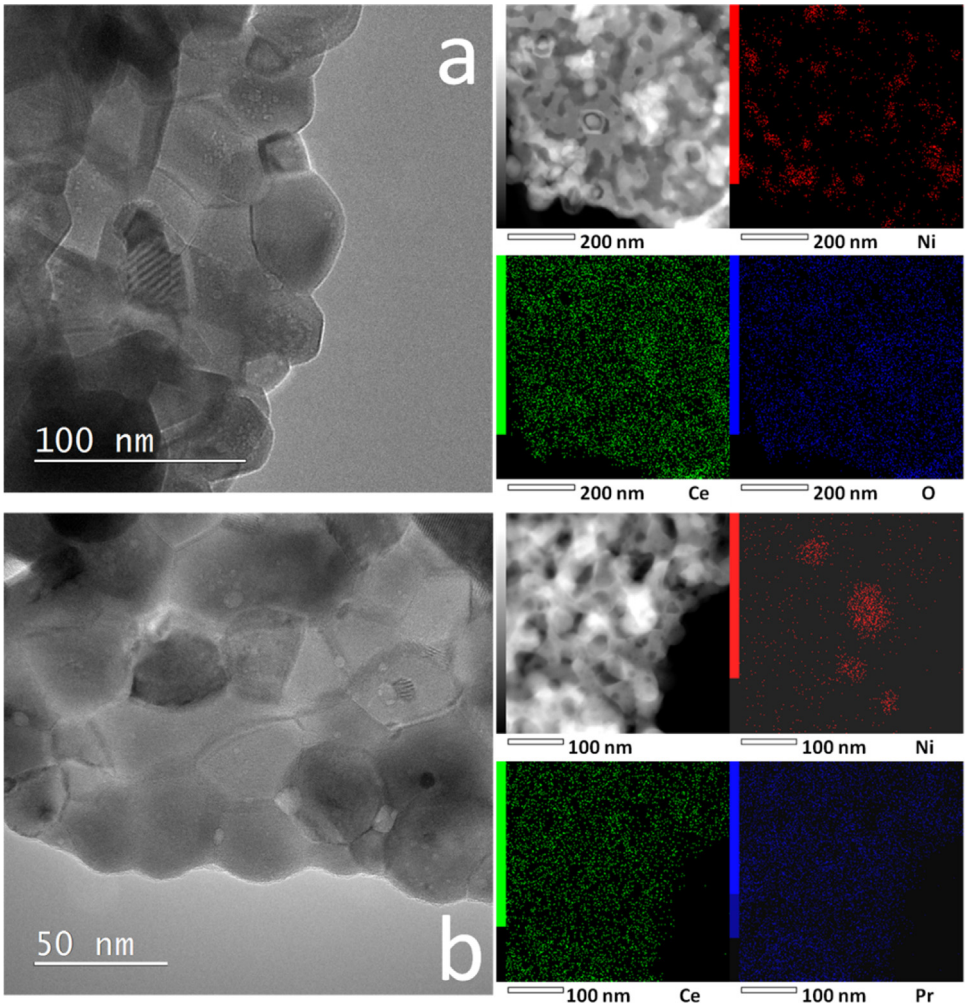

Fig. 1. TEM (left-hand side) and HAADF/STEM micrographs (right-hand side) with corresponding EDXS elemental mapping for (a) 5 wt% Ni/CeO_2 and (b) 5 wt% Ni/$Ce_{0.2}Pr_{0.8}O_{2-\delta}$ catalysts.

Table 1
H_2 desorption (μmol g^{-1}), Ni dispersion (D_{Ni}, %) and Ni mean particle size (d_{Ni}, nm) obtained by H_2-TPD performed on fresh 5 wt% Ni/$Ce_{1-x}Pr_xO_{2-\delta}$ (x = 0.0, 0.2, 0.5, 0.65, 0.8) catalysts. T_M (°C) is the temperature at which maximum H_2 desorption rate occurs.

Catalyst	T_M (°C)	H_2 (μmol g^{-1})	D_{Ni} (%)	d_{Ni} (nm)
5 wt%Ni/CeO_2	62, 138			
	232, 327	13.1	3.0	31.4
5 wt%Ni/$Ce_{0.8}Pr_{0.2}O_2$	64, 143			
	202, 368	10.0	2.8	34.4
5 wt%Ni/$Ce_{0.5}Pr_{0.5}O_2$	80, 218			
	255, 360	13.5	3.2	30.5
5 wt%Ni/$Ce_{0.35}Pr_{0.65}O_2$	86, 214			
	297	12.7	3.0	32.6
5 wt%Ni/$Ce_{0.2}Pr_{0.8}O_2$	86, 167			
	298	15.9	3.7	26.2

ciated Ni dispersion (D_{Ni}, %) are reported in Table 1 along with the peak maximum desorption temperatures (T_M,°C) observed. The good agreement between H_2 chemisorption (mean Ni particle size (d_{Ni}), Table 1) and powder XRD (mean NiO particle size, Table S1) is noted. According to the results of Fig. 2 and Table 1, the Pr/(Ce + Pr) % composition in support has largely influenced the heterogeneity of the Ni surface (e.g. E_{Ni-H} bond strength (T_M)) and the distribution of Ni_s hydrogen chemisorption sites. On the other hand, Ni dispersion and mean particle size remain practically similar (small variations of less than 12%) except for Ni/$Ce_{0.2}Pr_{0.8}O_{2-\delta}$ (~15–25% variation). In particular, the dispersion of Ni was found to be in the 2.8–3.7% range and the estimated Ni particle size in the 26–34 nm range. Ni/$Ce_{0.2}Pr_{0.8}O_{2-\delta}$ shows the highest Ni dispersion (smallest particle size), whereas Ni/$Ce_{0.8}Pr_{0.2}O_{2-\delta}$ the lowest one (largest particle size). The latter shows significantly higher activity but larger quantities of inactive "carbon" than Ni/$Ce_{0.2}Pr_{0.8}O_{2-\delta}$.

As Pr-dopant is progressively added in the ceria lattice (e.g. from 0 to 20 and 80 atom-%), the low-temperature (<150 °C) desorbing states (μmol H g^{-1}) of chemisorbed hydrogen (lower binding energy) decrease, whereas those at T > 150 °C increase. At least three main desorption states might be present in all three catalysts. H_2-TPD traces similar to those of Fig. 2 have been reported for the 15 wt% Ni/$Ce_{0.12}Zr_{0.88}O_2$ [38], 5 wt% Ni/$Ce_{1-x}Zr_xO_2$ [25,39], 5 wt% Ni/$Ce_{0.8}Pr_{0.2}O_2$ [25] and 5 wt% Ni/Al_2O_3—CaO [28] solids.

3.4. Catalytic performance studies

Fig. 3 reports on the catalytic performance of 5 wt% Ni/$Ce_{1-x}Pr_xO_{2-\delta}$ solids in the dry reforming of methane (550–750 °C) after 30 min on stream, in terms of CH_4 conversion (X_{CH4}, %) and H_2-yield (%) (Fig. 3A), CO_2 conversion (X_{CO2}, %) and CO-yield (%) (Fig. 3B) and H_2/CO gas-product ratio (Fig. 3C). It should be noted that no C_2H_6 was formed within the temperature

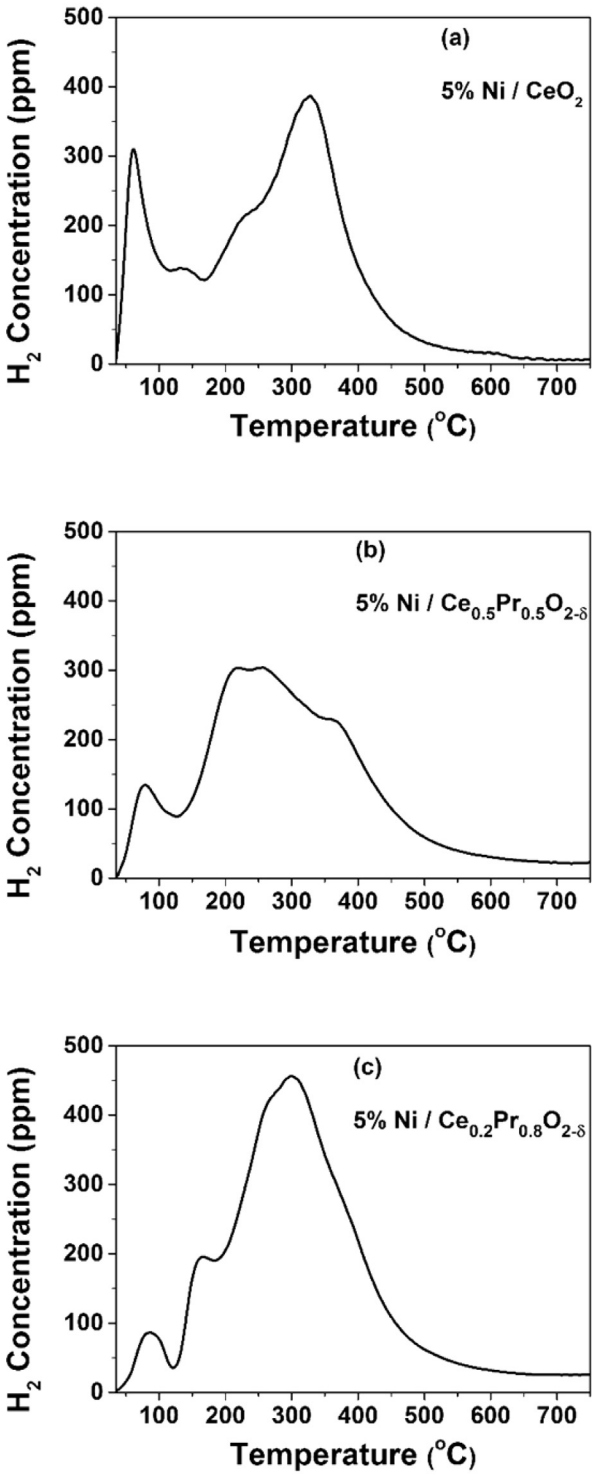

Fig. 2. H_2-TPD traces obtained over 5 wt% $Ni/Ce_{1-x}Pr_xO_{2-\delta}$ (x = 0, 0.5, 0.8) catalysts. F_{He} = 50 N mL/min; β=30 °C min^{-1}; W = 0.5 g.

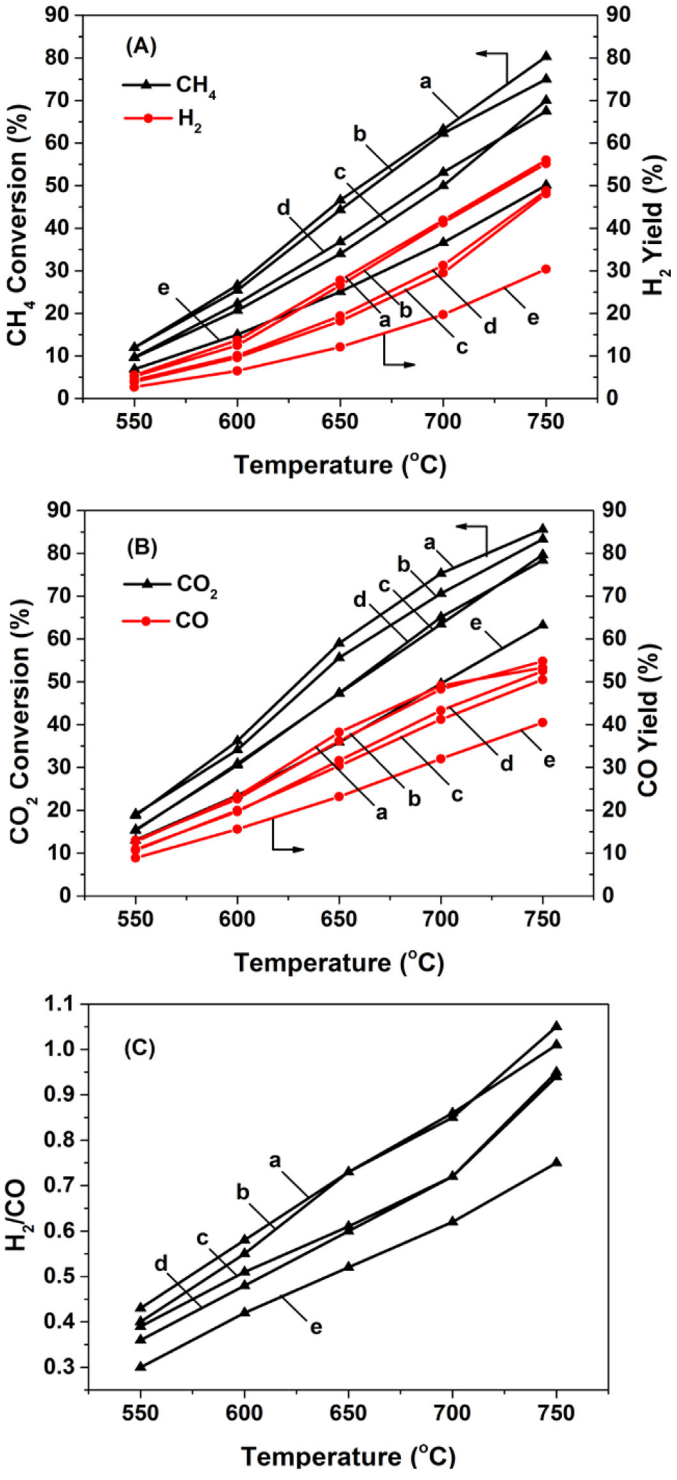

Fig. 3. (A) CH_4-conversion (%) and H_2 yield (%), (B) CO_2-conversion (%) and CO yield (%) and (C) H_2/CO gas-product ratio obtained after 30 min in dry reforming of methane in the 550–750 °C range over 5 wt% Ni supported on (a) CeO_2; (b) $Ce_{0.8}Pr_{0.2}O_{2-\delta}$; (c) $Ce_{0.5}Pr_{0.5}O_{2-\delta}$; (d) $Ce_{0.35}Pr_{0.65}O_{2-\delta}$ and (e) $Ce_{0.2}Pr_{0.8}O_{2-\delta}$ catalysts; P_{CH4} = 0.2 bar, P_{CO2} = 0.2 bar, P_T = 1.0 bar; GHSV = 30,000 h^{-1}.

range of 550–750 °C. By increasing the reaction temperature from 550 to 750 °C the catalytic activity increases considerably according to the endothermic nature of the reaction. For example, in the case of Ni/CeO_2, X_{CH4} increases from 12.0 to 80.3%. In all catalytic systems the CO_2-conversion (%) is found to be larger than that of CH_4-conversion (%) in the temperature range of 550–750 °C. The H_2/CO gas-product ratio takes low values in the 550–600 °C range (ca. 0.3–0.58) for all catalytic systems but significantly larger values (0.72–1.05) at 700 and 750 °C except for the 5 wt% $Ni/Ce_{0.2}Pr_{0.8}O_{2-\delta}$ (H_2/CO = 0.62–0.75). Table S2 (Supplementary information) provides all catalytic behaviour results of 5 wt% $Ni/Ce_{1-x}Pr_xO_{2-\delta}$ shown in Fig. 3. Dry reforming of CH_4 at 750 °C over the $Ce_{1-x}Pr_xO_{2-\delta}$ supports alone showed very small catalytic activity. In particular, $Ce_{0.8}Pr_{0.2}O_{2-\delta}$ resulted in X_{CO2} = 0.2%, X_{CH4} = 0.1% and CO- and H_2-yields of 1.25 and 0.1%, respectively. The effect of Pr-dopant on the stability (25 h on stream) of 5 wt%

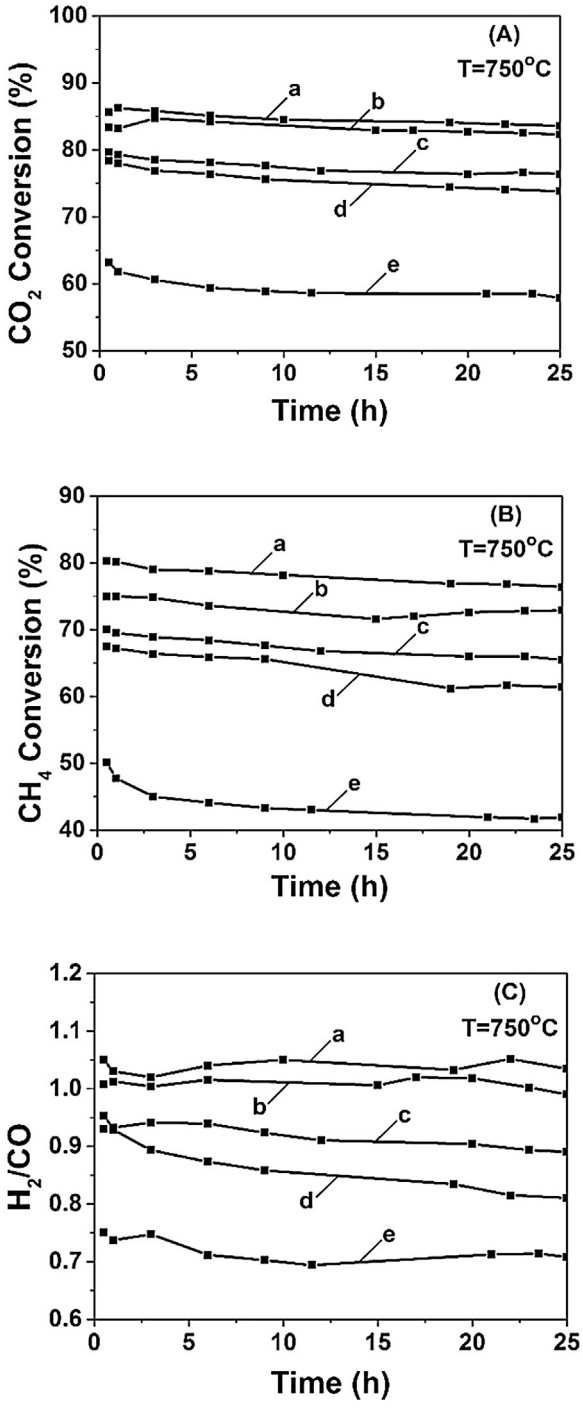

Fig. 4. Stability test (25 h) in the dry reforming of methane reaction performed at 750 °C in terms of CO_2-conversion (%) (A), CH_4-conversion (%) (B) and H_2/CO gas-product ratio (C) over 5 wt% Ni supported on (a) CeO_2; (b) $Ce_{0.8}Pr_{0.2}O_{2-\delta}$; (c) $Ce_{0.5}Pr_{0.5}O_{2-\delta}$; (d) $Ce_{0.35}Pr_{0.65}O_{2-\delta}$ and (e) $Ce_{0.2}Pr_{0.8}O_{2-\delta}$ catalysts; P_{CH4} = 0.2 bar, P_{CO2} = 0.2 bar, P_T = 1.0 bar; GHSV = 30,000 h^{-1}.

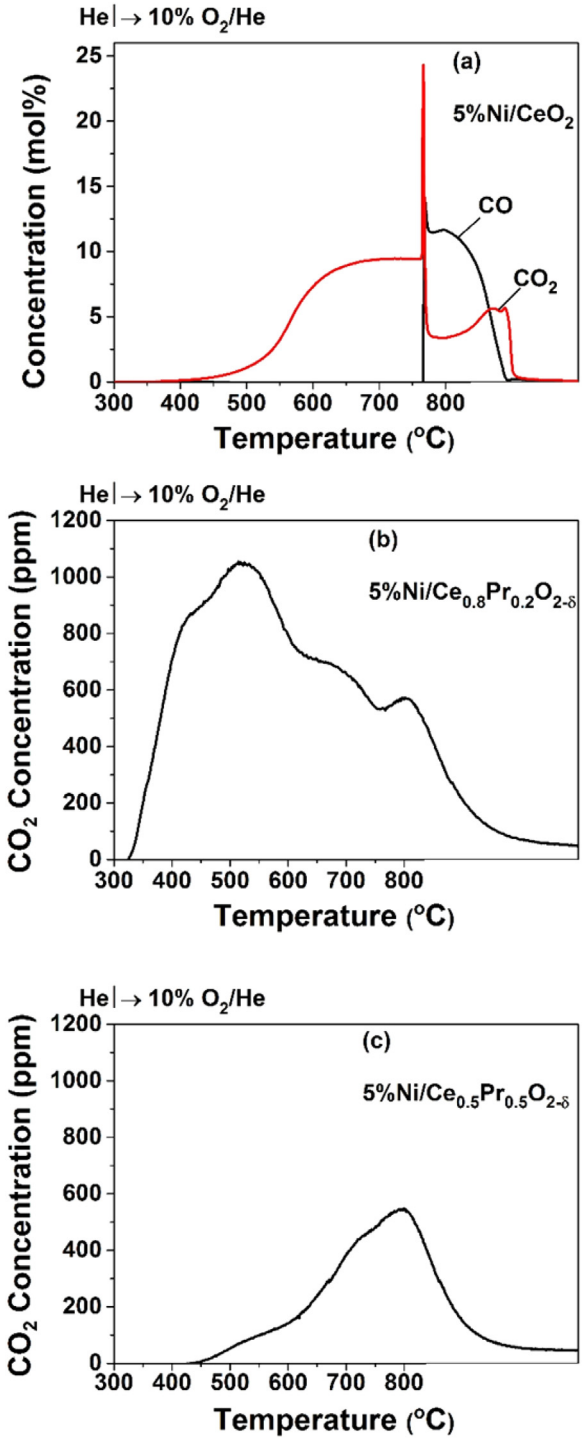

Fig. 5. Transient response curves of CO_2 and CO obtained during TPO of "carbon" formed after 25 h of dry reforming of methane at 750 °C (GHSV = 30,000 h^{-1}) over 5 wt% $Ni/Ce_{1-x}Pr_xO_{2-\delta}$ (x = 0.0, 0.2, 0.5) catalysts. Gas delivery sequence: DRM (750 °C, 25 h) → He, increase T to 800 °C until no CO and CO_2 are measured in the MS → cool down in He flow to 300 °C → T is increased to 800 °C (β = 30 °C min^{-1}).

$Ni/Ce_{1-x}Pr_xO_{2-\delta}$ solids at 750 °C is shown in Fig. 4. A monotonic %-drop in activity with increasing Pr-dopant concentration in the 50–80 atom-% range is obtained; 6.5–16.5% for CH_4 conversion and 4.0–8.5% for CO_2 conversion. On the other hand, the undoped and 20 atom-% Pr-doped ceria showed similar activity drop (3 and 5% for CH_4 conversion; 1.5 and 2.5% for CO_2 conversion, respectively).

An increasing concentration of Pr-dopant in the ceria matrix causes a continuous decrease of CH_4- and CO_2-conversion (%) and also of H_2/CO gas-product ratio, after 0.5 h or 25 h of DRM at 750 °C (Fig. S8, Supplementary information). In particular, CH_4-conversion, CO_2-conversion and H_2/CO gas-product ratio were lower by 37.5, 22.4 and 32.4%, respectively, when Ni/CeO_2 and $Ni/Ce_{0.2}Pr_{0.8}O_{2-\delta}$ solids are compared after 0.5 h of reaction. This monotonic loss of activity with increasing Pr-dopant concentration in the $Ce_{1-x}Pr_xO_{2-\delta}$ support is not due to the accumulation of inactive "carbon" since the latter shows a remarkable decrease with increasing concentration of Pr-dopant in the support (Section 3.5).

Table 2
Temperature-programmed oxidation (TPO) of "carbon" (CO and CO_2 formation, μmol g^{-1}) formed after 25 h of DRM at 750 °C over 5 wt% $Ni/Ce_{1-x}Pr_xO_{2-\delta}$ (x = 0.0, 0.2, 0.5, 0.8) catalysts (see Section 2.4.1). The amount of "carbon" (wt%) measured by TGA-TPO is also reported.

Catalyst	CO (μmol g^{-1})	CO_2 (μmol g^{-1})	"Carbon" (μmol g^{-1})[a]	"Carbon" (wt%) TGA-TPO[b]
5 wt%Ni/CeO_2	4627	11,727	16,354 (19.6)[c]	37.7
5 wt%$Ni/Ce_{0.8}Pr_{0.2}O_2$	–[d]	182	182 (0.22)	29.9
5 wt%$Ni/Ce_{0.5}Pr_{0.5}O_2$	–	64.5	64.5 (0.08)	0.90
5 wt%$Ni/Ce_{0.2}Pr_{0.8}O_2$	–	58.3	58.3 (0.07)	0.15

[a] DRM reaction conditions: catalytic bed: 0.15 g catalyst + 0.15 g SiC; total flow rate: 150 N mL/min.
[b] DRM reaction conditions: catalytic bed: 0.3 g catalyst, no SiC; total flow rate: 150 N mL/min.
[c] wt% "carbon".
[d] No CO is observed.

3.5. Characterisation of "carbon" formed during DRM by various transient techniques

3.5.1. Temperature programmed oxidation (TPO)

Fig. 5 presents CO_2 and CO traces of temperature-programmed oxidation (TPO) of "carbon" obtained over the 5 wt% $Ni/Ce_{1-x}Pr_xO_{2-\delta}$ (x = 0.0, 0.2 and 0.5) catalysts after 25 h of DRM at 750 °C. The amount of "carbon" formed and the rate (proportional to the gas phase concentration) vs. temperature profiles are strongly influenced by the Pr-dopant concentration in the support. A notably different feature of TPO trace is observed in the case of 5 wt% Ni/CeO_2 when compared to the other two catalysts' compositions. The sharp increase in the rate of "carbon" oxidation to CO_2 which occurred at ~760 °C and the trace of CO starting at temperatures higher than ~760 °C for the case of Ni/CeO_2, which are absent in the case of $Ni/Ce_{1-x}Pr_xO_{2-\delta}$ catalysts (x = 0.2 and 0.5) are noted. These TPO traces probe for various kinds of "carbon" with different distribution based on the temperature at which maximum oxidation rate occurs. The kinetics of oxidation of these kinds of "carbon" is apparently influenced by the Pr-dopant in the support, where low Pr-dopant loadings result in a type of "carbon" more easily oxidized compared to that obtained with larger Pr-dopant loadings (e.g. 80 atom-%). Table 2 reports the total amount of "carbon" (μmol C g^{-1} and wt% C) measured by TPO after 25 h of DRM over the 5 wt% $Ni/Ce_{1-x}Pr_xO_{2-\delta}$ catalysts. A remarkable reduction in "carbon" deposition is obtained when ceria is doped with 80 atom-% Pr, namely 19.6 wt% C for Ni/CeO_2 to be compared with 0.07 wt% C for the $Ni/Ce_{0.2}Pr_{0.8}O_{2-\delta}$ catalyst.

The remarkable support effect in the reduction of the rate of "carbon" deposition due to Pr-doped ceria support in the DRM over the 5 wt% $Ni/Ce_{1-x}Pr_xO_{2-\delta}$ catalysts was also investigated at higher CH_4 and CO_2 conversions than those reported in Fig. 4A and B after using 0.3 g of catalyst (no SiC was used) and a flow rate of 150 NmL/min; after 25 h of dry reforming, CH_4-conversions 55–87% and CO_2-conversions 70–92% were obtained. The "carbon" accumulated was measured by TGA-TPO and CHNS techniques and results are presented in Fig. S9 (Supplementary information). According to the TGA analysis 5 wt% Ni/CeO_2 accumulated 37.7 wt% carbon. When Pr-dopant was introduced into the ceria lattice at the level of 20, 50, 65 and 80 atom-%, the amount of carbon decreased to 29.9, 0.9, 13.2 and 0.1 wt%, respectively. It appears that the extent of "carbon" accumulation is influenced significantly by the CH_4- and CO_2-conversion levels.

3.5.2. Scanning electron microscopy (SEM)

SEM micrographs of fresh and spent (after 25 h of DRM at 750 °C) catalysts samples are illustrated in Fig. 6a–e. The supports of all five fresh catalysts consist of particles in the 50–150 nm range in size, which are agglomerated into larger porous structures. In the case of spent 5 wt% $Ni/Ce_{0.5}Pr_{0.5}O_{2-\delta}$ and 5 wt% $Ni/Ce_{0.2}Pr_{0.8}O_{2-\delta}$ catalysts (Fig. 6c and e), hardly any carbon filaments could be observed. On the other hand, in the other spent catalysts the amount of carbon deposits was significantly larger, result that was confirmed by means of SEM analyses, where numerous carbon filaments were observed. Graphitic carbon has also been identified on the spent 5 wt% Ni/CeO_2 catalyst by XRD as shown in Fig. S10 (Supplementary information).

3.5.3. Quantifying the origin of "carbon" formation (CH_4 vs. CO_2 activation route)

Fig. 7 presents $^{12}CO_2$ and $^{13}CO_2$ transient response curves recorded during TPO of the "carbon" formed over the 5 wt% $Ni/Ce_{1-x}Pr_xO_{2-\delta}$ (x = 0.0 and 0.8) catalysts after 30 min of dry reforming (5%$^{13}CO_2$/5%$^{12}CH_4$/He) at 550 and 750 °C (see Section 2.5). The different shape and position in the obtained $^{13}CO_2$ and $^{12}CO_2$ response curves for the two catalysts and their relative amounts (area under the TPO trace) are apparent. In the case of DRM at 550 °C over Ni/CeO_2 both $^{13}CO_2$ and $^{12}CO_2$ traces exhibit a main peak centred at ~545 °C (Fig. 7a) and a shoulder at the falling part (~620 °C). On the other hand, in the case of $Ni/Ce_{0.2}Pr_{0.8}O_{2-\delta}$ both $^{13}CO_2$ and $^{12}CO_2$ traces consist only of one symmetrical peak centred at ~575 °C (Fig. 7c). A similar behaviour is also observed when DRM was performed at 750 °C (Fig. 7d) but a slightly different behaviour is seen in the case of Ni/CeO_2 (Fig. 7b). For the latter catalyst maximum oxidation rate occurs at ~630 °C, which is higher than that occurred after DRM at 550 °C (Fig. 7a). In the case of $Ni/Ce_{0.2}Pr_{0.8}O_{2-\delta}$ the rate maximum occurred at the same temperature (Fig. 7c, d). These results imply that Pr-dopant in the support likely influences the type of "carbon" deposited as a function of DRM reaction temperature. The $^{13}CO_2$-TPO traces arise from the oxidation of ^{13}C-containing "carbon" formed via the $^{13}CO_2$ activation route, whereas those of $^{12}CO_2$ from the oxidation of ^{12}C-containing "carbon" formed via the $^{12}CH_4$ decomposition route.

Table 3 reports the amounts (μmol g^{-1} and wt% C) of $^{12}CO_2$, $^{13}CO_2$ and total "carbon", the $^{12}CO_2/^{13}CO_2$ ratio and the %-contribution of the CO_2 activation route to total "carbon" deposition

Table 3
$^{12}CO_2$ and $^{13}CO_2$ (μmol g^{-1}) and $^{12}CO_2/^{13}CO_2$ product ratio obtained during temperature-programmed oxidation (TPO) of "carbon" formed after 30 min of dry reforming (5%$^{13}CO_2$/5%$^{12}CH_4$/45%/Ar/45%He) at 550 and 750 °C over 5 wt% Ni/CeO_2 and 5 wt% $Ni/Ce_{0.2}Pr_{0.8}O_{2-\delta}$ catalysts. DRM reaction conditions: F_T = 100 N mL/min; W_{cat} = 0.2 g (no SiC as dilution was used).

Catalyst	T (°C)	$^{12}CO_2$ (μmol g^{-1})	$^{13}CO_2$ (μmol g^{-1})	$^{12}CO_2/^{13}CO_2$	Total "carbon"
5 wt% Ni/CeO_2	550	593.6	1139.6	0.52 (65.7)[a]	1733.2 (2.08)[b]
	750	984.8	1158.3	0.87 (54.0)	2143.1 (2.57)
5 wt% $Ni/Ce_{0.2}Pr_{0.8}O_{2-\delta}$	550	75.9	114.5	0.66 (60.1)	190.4 (0.23)
	750	153.7	159.1	0.96 (50.9)	312.8 (0.38)

[a] %-contribution of the CO_2 activation route to the total "carbon" derived from both CH_4 and CO_2 activation routes.
[b] wt% "carbon".

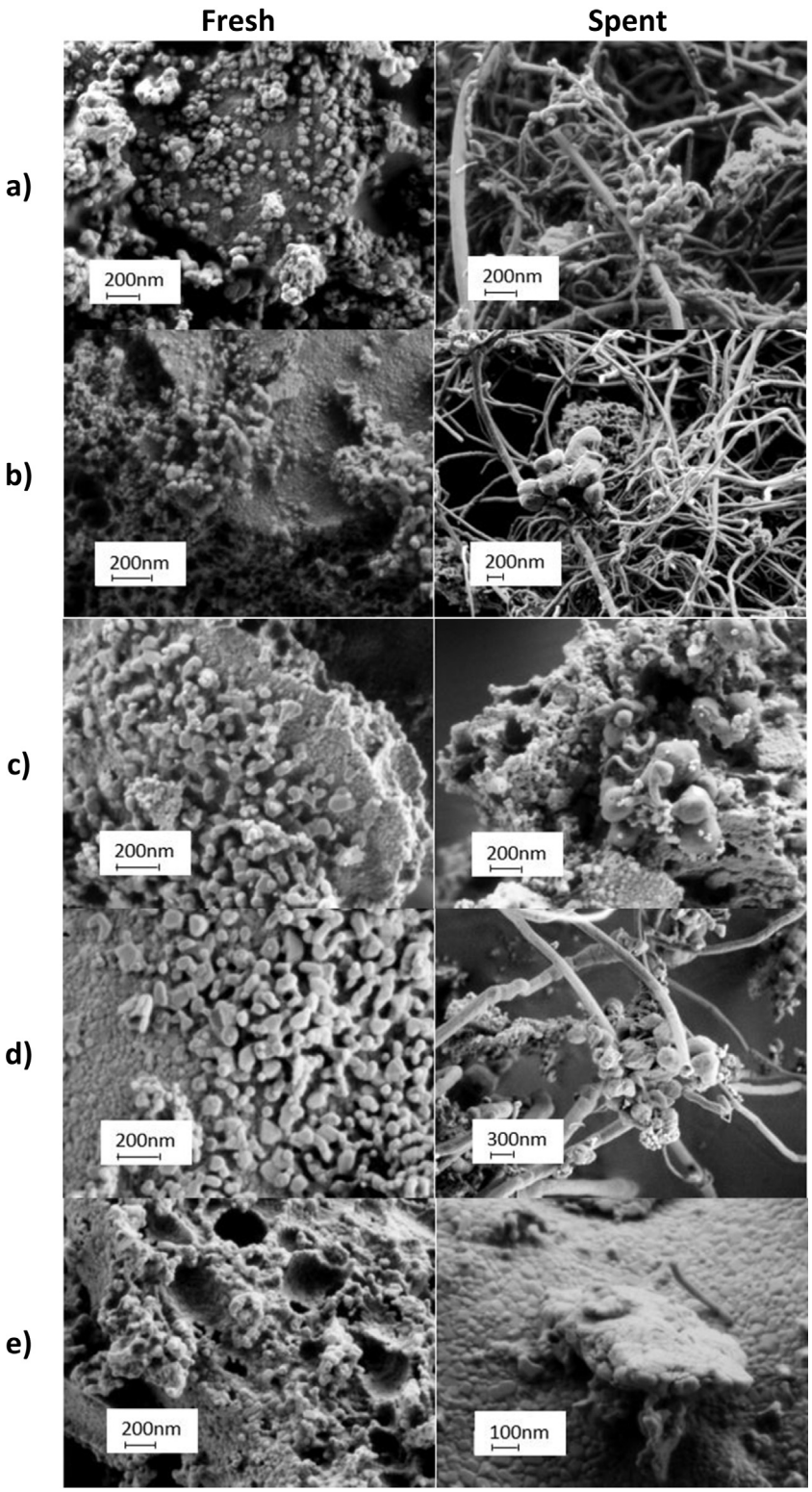

Fig. 6. SEM micrographs obtained on the fresh and spent (after 25 h on stream in DRM at 750 °C) catalysts: (a) 5 wt% Ni/CeO_2, (b) 5 wt% $Ni/Ce_{0.8}Pr_{0.2}O_{2-\delta}$, (c) 5 wt% $Ni/Ce_{0.5}Pr_{0.5}O_{2-\delta}$, (d) 5 wt% $Ni/Ce_{0.35}Pr_{0.65}O_{2-\delta}$ and (e) 5 wt% $Ni/Ce_{0.2}Pr_{0.8}O_{2-\delta}$.

after DRM at 550 and 750 °C over the undoped and 80 atom-% doped ceria supported Ni catalysts. At the lowest T of 550 °C, after increasing the Pr-dopant concentration from zero (Ni/CeO_2) to 80 atom-% ($Ni/Ce_{0.2}Pr_{0.8}O_{2-\delta}$), the deposited "carbon" is found to largely decrease to a very low value (0.06 wt% or 60 mg g_{cat}^{-1}). In contrast, the Pr-dopant concentration affects only to a small extent the %-contribution of the CO_2 activation route to "carbon" deposition (e.g. 50.9% for $Ni/Ce_{0.2}Pr_{0.8}O_{2-\delta}$ and 54% for Ni/CeO_2 at 750 °C). For these particular catalytic systems, it is clear that the CO_2 activation route becomes to a large extent dominant for the deposition of *inactive* "carbon" at 550 °C. However, at 750 °C the inactive "carbon" derived from the CH_4 decomposition route becomes equally

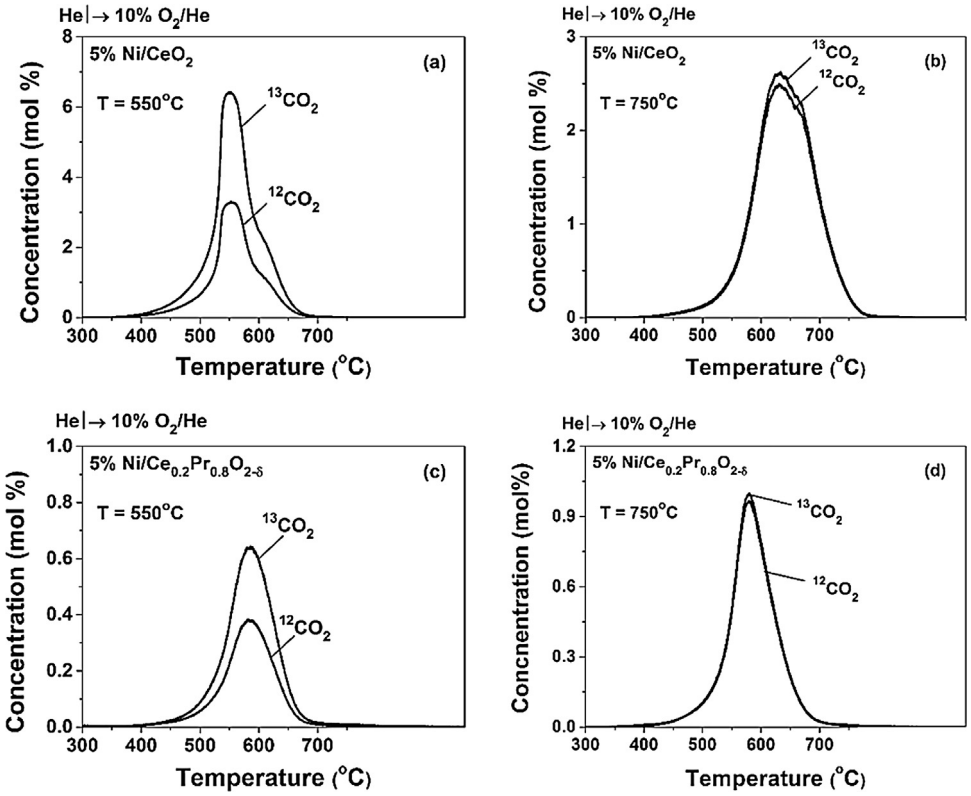

Fig. 7. Temperature-programmed oxidation (TPO) of "carbon" formed during dry reforming of $^{12}CH_4$ with $^{13}CO_2$ at 550 and 750 °C over 5 wt% Ni/CeO_2 (a, b) and 5 wt% $Ni/Ce_{0.2}Pr_{0.8}O_{2-\delta}$ (c, d) catalysts. Gas delivery sequence: 5%$^{13}CO_2$/5%$^{12}CH_4$/Ar/He (T, 30 min, F_T = 100 N mL min^{-1}) → He (750 °C, 10 min) → cool in He flow to 100 °C → 10%O_2/He, TPO (F_T = 50 N mL min^{-1}, β=30 °C min^{-1}); W = 0.2 g (fresh catalyst).

Table 4
Steady-state concentrations (μmol g^{-1} or θ) of active "carbon" (N_C) and reversibly adsorbed CO_2 (N_{CO2}, μmol g^{-1} or θ) measured by SSITKA after 2 h of dry reforming (5%CH_4/5%CO_2/He) at 550 and 750 °C.

Catalyst	T (°C)	N_C (μmol g^{-1})	N_{CO2} (μmol g^{-1})	τ_C (s)	$TOF_{ITK,CO}$ (s^{-1})	$Rate_{CO/CO2}$[b] (μmol g^{-1} s^{-1})	X_{CO2} (%)	X_{CH4} (%)
5 wt%	550	3.7 (0.15)[a]	38.0 (1.5)[a]	0.60	1.7	6.30	14.0	9.0
Ni/CeO_2	750	87.7 (3.40)	54.7 (2.3)	1.74	–		62.4	53.7
5 wt%	550	0.72 (0.025)	35.9 (1.45)	0.11	9.1	6.55	11.5	8.4
$Ni/Ce_{0.8}Pr_{0.2}O_2$	750	2.0 (0.07)	86.8 (3.6)	0.06	–		36.0	32.0
5 wt%	550	0.87 (0.03)	57.6 (2.1)	0.20	5.0	4.35	5.8	4.1
$Ni/Ce_{0.2}Pr_{0.8}O_2$	750	16.7 (0.56)	114.0 (4.05)	0.78	1.3		15.8	14.7

[a] Number in parentheses represents the equivalent surface coverage (θ) based on Ni_s (Table 1).
[b] Rate of CO formation via the CO_2 activation route (Eq. (9)).

important. We have recently reported [25] that part of the CO formed in dry reforming over 5 wt% $Ni/Ce_{0.8}Pr_{0.2}O_{2-\delta}$ leads to the formation of *inactive* carbon via the Boudouard reaction.

3.6. Measurement of active carbon derived from the CO_2 activation route (SSITKA)

Fig. 8 shows transient response curves (in terms of a dimensionless Z concentration function) for Kr (tracer gas), ^{13}CO and $^{13}CO_2$ during the SSITKA switch $^{12}CH_4$/$^{12}CO_2$/Ar/He (2 h) → $^{12}CH_4$/$^{13}CO_2$/Ar/Kr/He (20 min) → $^{12}CH_4$/$^{12}CO_2$/Ar/He (t) at 750 °C over the most active 5 wt% Ni/CeO_2 (Fig. 8a) and the least active 5 wt% $Ni/Ce_{0.2}Pr_{0.8}O_{2-\delta}$ (Fig. 8b) catalysts (see Figs. 3 and 4). It is seen that for both catalysts the ^{13}CO response curve lags behind that of $^{13}CO_2$ and the latter response lags behind that of Kr tracer gas (characteristic response for a non-adsorbing and non-reacting gas). The exchange of the *active* "carbon" pool lasts about 90 and 40 s for the Ni/CeO_2 (Fig. 8a) and $Ni/Ce_{0.2}Pr_{0.8}O_{2-\delta}$ (Fig. 8b) catalysts, respectively. After applying the material balance Eq. (6), the amount of *active* "carbon" can be estimated and values are reported in Table 4 for Ni/CeO_2, $Ni/Ce_{0.8}Pr_{0.2}O_{2-\delta}$ and $Ni/Ce_{0.2}Pr_{0.8}O_{2-\delta}$ catalysts; the equivalent number of surface monolayers based on the Ni surface (Table 1, D_{Ni} (%)) and after assuming C/Ni_s = 1 is also reported. As Pr-dopant increases from zero (undoped ceria) to 80 atom-%, the active "carbon" concentration decreases. More precisely, values of 87.7 (θ_c = 3.4), 2.0 (θ_c = 0.07) and 16.7 μmol/g (θ_c = 0.56) are obtained for the Ni/CeO_2, $Ni/Ce_{0.8}Pr_{0.2}O_{2-\delta}$ and $Ni/Ce_{0.2}Pr_{0.8}O_{2-\delta}$ catalysts, respectively. It should be noted that these values correspond to integral reaction conditions (CO_2 conversions in the 16–62% range).

The amount (N_{CO2}, μmol g^{-1}) of reversibly adsorbed CO_2 formed on the catalyst surface after 2 h of DRM and which does not participate in the formation of CO is estimated via Eq. (7) and reported in Table 4. As opposed to the case of *active* "carbon" pool (Scheme 1), the progressive increase of Pr-dopant loading in catalyst's support composition causes also a progressive increase in the amount of reversibly adsorbed CO_2 at 750 °C. This is found to be 54.7 (θ = 2.3), 86.8 (θ = 3.6) and 114.0 μmol/g (θ = 4.05), respectively, for the Ni/CeO_2, $Ni/Ce_{0.8}Pr_{0.2}O_{2-\delta}$ and $Ni/Ce_{0.2}Pr_{0.8}O_{2-\delta}$ catalysts. It is very important to point out that the size of this reversibly adsorbed

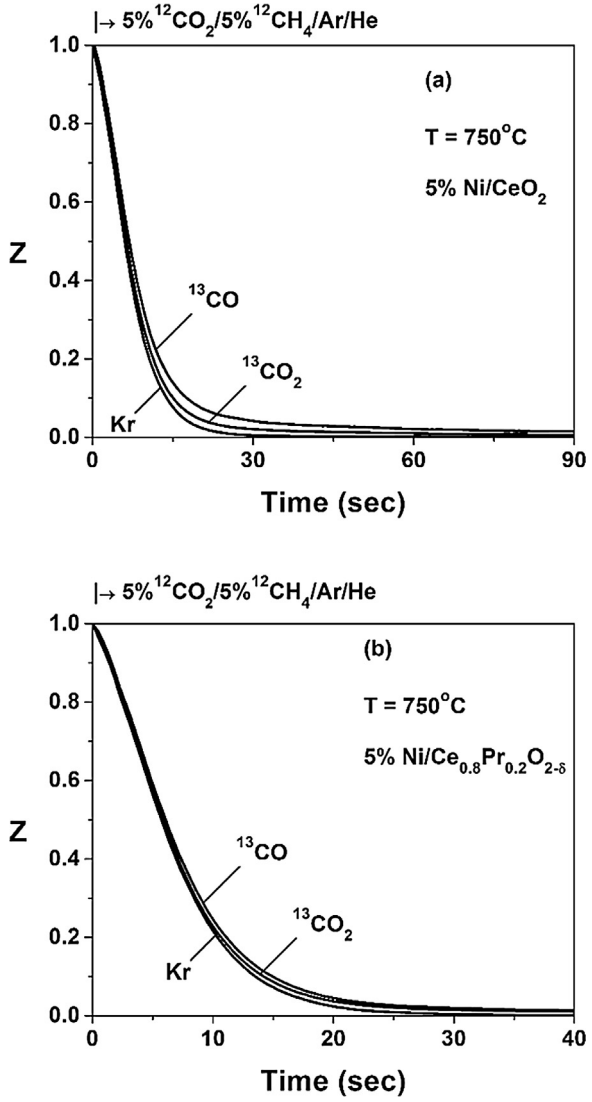

Fig. 8. Kr, ^{13}CO and $^{13}CO_2$ SSITKA response curves obtained after 2 h of dry reforming of methane at 750 °C over (a) 5 wt% Ni/CeO_2 and (b) 5 wt% $Ni/Ce_{0.8}Pr_{0.2}O_{2-\delta}$ catalysts. SSITKA switches: $5\%^{12}CO_2/5\%^{12}CH_4/Ar/He$ (2 h) → $5\%^{13}CO_2/5\%^{12}CH_4/2\%Kr/Ar/He$ (20 min) → $5\%^{12}CO_2/5\%^{12}CH_4/Ar/He$ (t); W_{cat} = 30 mg diluted with 0.17 g SiC; F_T = 100 N mL min^{-1}.

CO_2 pool is larger than one monolayer of Ni surface. On the other hand, the size of the *active* C-pool that leads to CO is lower than one monolayer except for the case of Ni/CeO_2 (θ_C = 3.4).

Similar SSITKA experiments to those shown in Fig. 8 were also performed at 550 °C and the obtained results are reported in Table 4. These SSITKA measurements correspond to truly kinetic conditions (CO_2 and CH_4 conversions lower than 15%) as opposed to the case at 750 °C. It is observed that practically the same behaviour in the concentration of active "carbon" and reversibly adsorbed CO_2 formed at 550 °C with increasing Pr-dopant loading is obtained as in the case of DRM at 750 °C. More precisely, the *active* "carbon" is 3.7 μmol/g for Ni/CeO_2, which is significantly reduced to 0.72 and 0.87 μmol/g for the $Ni/Ce_{0.8}Pr_{0.2}O_{2-\delta}$ and $Ni/Ce_{0.2}Pr_{0.8}O_{2-\delta}$ catalysts, respectively. Similarly, the reversibly adsorbed CO_2 is 38.0 μmol/g for the Ni/CeO_2 and increases to 57.6 μmol/g for the $Ni/Ce_{0.2}Pr_{0.8}O_{2-\delta}$ catalyst. A slightly lower value was estimated for $Ni/Ce_{0.8}Pr_{0.2}O_{2-\delta}$ (35.9 μmol g^{-1}). The influence of reactant conversion on the concentration of *active* C-pool and that of *reversibly adsorbed* CO_2 was also investigated at 550 °C. Fig. 9 shows SSITKA transient response curves for Kr, ^{13}CO and $^{13}CO_2$ obtained over 5 wt% Ni/CeO_2 at 550 °C

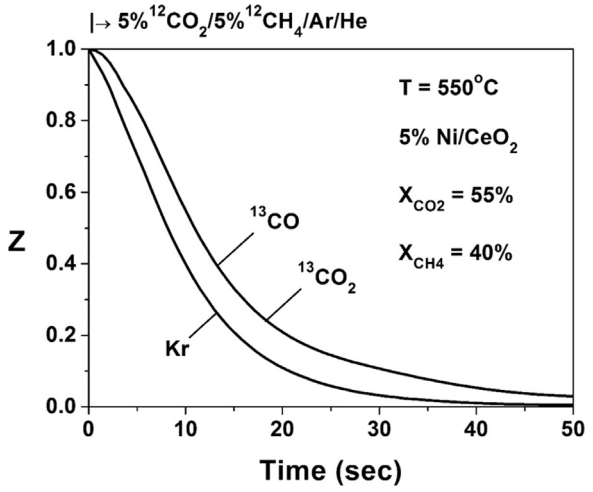

Fig. 9. Kr, ^{13}CO and $^{13}CO_2$ SSITKA response curves obtained after 2 h in dry reforming of methane at 550 °C over 5 wt% Ni/CeO_2 catalyst. SSITKA switches: $5\%^{12}CO_2/5\%^{12}CH_4/Ar/He$ (2 h) → $5\%^{13}CO_2/5\%^{12}CH_4/2\%Kr/Ar/He$ (20 min) → $5\%^{12}CO_2/5\%^{12}CH_4/Ar/He$ (*t*); W_{cat} = 0.25 g; F_T = 50 NmL min^{-1}; X_{CH4} = 40%; X_{CO2} = 55%.

for CO_2- and CH_4-conversion levels of 55 and 40%, respectively, after 2 h of DRM. The *active* "carbon" (N_C) formed was ~ 2 μmol g^{-1} to be compared to the value of 3.7 μmol g^{-1} obtained at low conversions (Table 4), while the amount of reversibly adsorbed CO_2 was 10.7 μmol g^{-1}.

Table 4 reports the mean-life time (τ_C, s) of all the *active* "carbon" reaction intermediates found in the CO_2 activation path (e.g. "C"-s and CO-s, Scheme 1) and how this is influenced by the reaction temperature and Pr concentration in the Pr-doped ceria supported Ni catalysts. Also, TOF_{ITK} (s^{-1}) values ($TOF_{ITK} = 1/\tau_C$) are reported (Table 4) for differential conditions at 550 °C and for the $Ni/Ce_{0.2}Pr_{0.8}O_{2-\delta}$ at 750 °C as well. It is clearly illustrated that $Ni/Ce_{0.8}Pr_{0.2}O_{2-\delta}$ shows a TOF_{ITK} value about *5 times larger* than that of Ni/CeO_2, where both catalysts show similar catalytic activity when this is expressed per gram of catalyst basis (Fig. 4). In the case of $Ni/Ce_{0.8}Pr_{0.2}O_{2-\delta}$ catalyst, the TOF_{ITK} at 750 °C is smaller by a factor of ~ 3.8 when compared to the value estimated at 550 °C. This result can be understood after considering that TOF_{ITK} might be seen as the product of N_C and k. The latter parameter represents the site reactivity of that active "carbon" species which is associated with the *rate-limiting step* found in the CO_2 activation path (Scheme 1) at a given reaction temperature. It appears that k has a lower value at 750 °C as opposed to 550 °C due to a change in the chemical structure of the "active" carbon species and/or to a change in the structure of the adsorbed phase, considering that N_C (associated with the rate-limiting step) is still larger at 750 than 550 °C. The importance of these TOF_{ITK} measurements is discussed below.

Fig. 10 presents the transient evolution of the rate of hydrogen formation (μmol H_2 g^{-1} s^{-1}) after the feed is switched from He to the non-isotopic $^{12}CO_2/^{12}CH_4/Ar/He$ feed gas composition over the fresh 5 wt% $Ni/Ce_{1-x}Pr_xO_{2-\delta}$ (x = 0, 0.2 and 0.8) catalysts at 550 °C (Fig. 10a) and 750 °C (Fig. 10b). Upon the switch to the reaction mixture the rate of reaction at 550 °C sharply increases and passes through a maximum at time t ~ 15 s, where quickly (after ~ 2 min on stream) reaches a steady-state value (Fig. 10a). Of interest is the fact that the overshoot observed falls with the increase in Pr-dopant concentration as shown in Fig. 10a. As the reaction temperature increases to 750 °C (Fig. 10b), no overshoot in the rate of H_2 formation is observed. In particular, Ni/CeO_2 and $Ni/Ce_{0.8}Pr_{0.2}O_{2-\delta}$ catalysts rapidly (after ~1 min) take a steady-state reaction rate value, which decreases only slightly for longer times on stream and for larger reactant concentrations in the feed stream

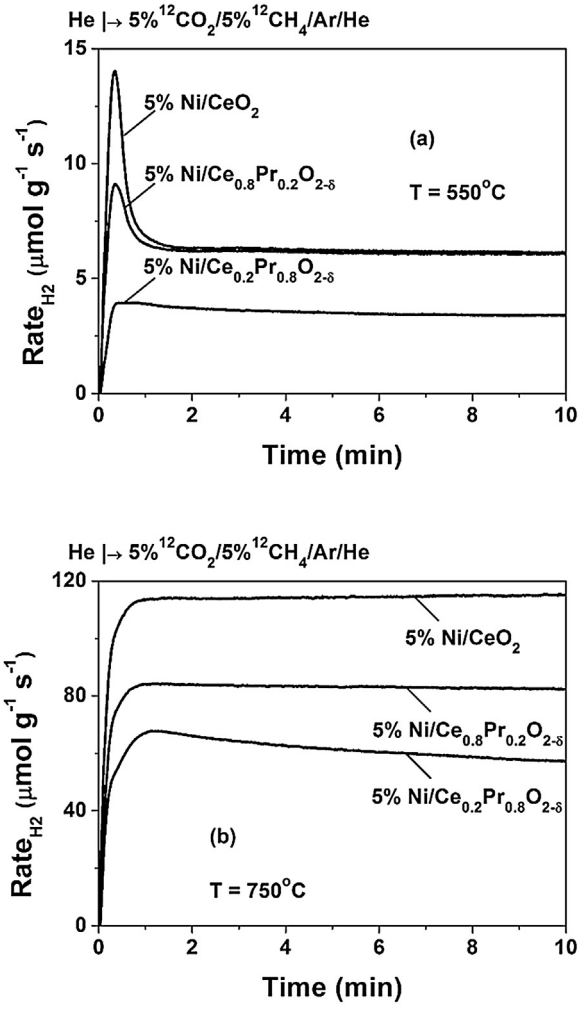

Fig. 10. Isothermal transient rates of hydrogen formation obtained at the switch He→ 5%$^{12}CO_2$/5%$^{12}CH_4$/Ar/He (t) at 550 °C (a) and 750 °C (b) over the 5 wt% $Ni/Ce_{1-x}Pr_xO_{2-\delta}$ (x = 0.0, 0.2 and 0.8) catalysts; W_{cat} = 0.1 g mixed with 0.1 g SiC (550 °C) and W_{cat} = 0.03 g mixed with 0.17 g SiC (750 °C); F_T = 100 N mL min^{-1}.

(see Fig. 3). The $Ni/Ce_{0.2}Pr_{0.8}O_{2-\delta}$ shows a small decay in the first 10-min of the transient (Fig. 10b) which is consistent also to the stability behaviour shown in Fig. 4.

4. Discussion

4.1. Catalytic performance of Ni/CeO_2 and $Ni/Ce_{1-x}Pr_xO_{2-\delta}$ solids

4.1.1. Ni/CeO_2

One of the earliest investigations [19] on the use of ceria as promoter of Ni for the dry reforming of methane has examined γ-Al_2O_3, CeO_2 and x wt% CeO_2-Al_2O_3 (x = 1–10 wt%) as supports of 5 wt% Ni. It was concluded that ceria produced strong metal-support interactions after calcination and H_2 reduction at 500 °C, which reduced the catalytic activity and carbon formation with respect to Ni/γ-Al_2O_3. On the other hand, when 1–5 wt% CeO_2 was deposited onto the alumina support this had a positive effect on the activity, stability and suppression of carbon deposition for the Ni/CeO_2-Al_2O_3 catalytic system. The stability and significant resistance to coking exhibited by the ceria-promoted nickel catalysts were attributed to the oxidative properties of CeO_2 along with the higher dispersions of Ni [19]. The amount of "carbon" deposited on Ni/γ-Al_2O_3, Ni/1wt%CeO_2-Al_2O_3 and Ni/CeO_2 solids was 20.8, 3.4 and 0.9 wt%, respectively, after 2 h of dry reforming (50 vol% CH_4, CH_4/CO_2 = 1) at 700 °C.

Asami et al. [40] in a later publication aimed at developing an excellent catalyst for dry reforming of methane by examining the possibility of using CeO_2 as support of Ni, Co and Fe. A 5.3 wt% Ni/CeO_2 (Ni dispersion of ~2.8%) was found to be the most effective catalyst (95% CH_4-conversion, H_2/CO ~1.0 and high stability after 50 h on reaction stream at 850 °C (50%CH_4/50%CO_2; W/F = 1 g h/mol)) with negligible carbon deposition. However, at 700 °C rapid deactivation of the catalyst occurred in agreement also to previous studies [41]. After using an equimolar feed gas composition the amount of "carbon" deposited after 24 h of reaction at 700 °C was 2 wt%, which was the lowest among the other investigated supported Ni catalysts (support: SiO_2, MgO, La_2O_3). Kumar et al. [16] have investigated CeO_2-ZrO_2 and ceria-doped ZrO_2 supported Ni (5 wt%) in an effort to evaluate how the catalytic activity of dry reforming and "carbon" formation are influenced by the support preparation method. The use of surfactant (CTAB) was one of the support synthesis methods used, which intended to lead to a reduction of the support's particle size into such an extent that it can become comparable to the Ni metal particle size, thus enabling strong metal-support interactions. A 5 wt% Ni/CeO_2 (CTAB) showed decreasing conversions up to 5 h on reaction stream, an H_2-selectivity of ~70% and ~1.1 wt% "carbon" deposition after only 3 h on reaction stream (40%CO_2/40%CH_4/20%N_2) at 700 °C.

Very recent works have investigated CeO_2 and ZrO_2-CeO_2 as supports of Ni for the dry reforming of methane [42,43]. Kim et al. [42] have investigated a 10 wt% Ni/CeO_2 (11.7 SSA, $m^2\,g^{-1}$) at 750 °C. A CH_4-conversion of 55%, a H_2/CO ratio of 0.73 and a very stable activity up to 10 h on stream (50%CH_4/50%CO_2) were reported. Deposited carbon in the shape of filamentous rods was also reported [42]. The H_2/CO ratio measured in the present 5 wt% Ni/CeO_2 catalyst is larger (close to unity) compared to the value of 0.73 reported [42]. The deviation of H_2/CO ratio from unity is discussed below.

Ay and Üner [43] have investigated the dry reforming of methane over a 8 wt% Ni/CeO_2 catalyst the support of which was prepared by the calcination of $Ce(C_2H_3O_2)_3 \cdot 1.5H_2O$ at 700 °C and using the same feed gas composition (20%CH_4/20%CO_2/Ar) and hydrogen reduction temperature (ca. 700 °C) as in the present work. A very similar catalytic behaviour to that reported in Fig. 4 was observed after 5 h on stream with respect to the level of reactant conversions and H_2/CO ratio. However, an initial deactivation of about 20% (up to 5 h on stream) was seen [43], opposite to that observed in the present work (Fig. 4B). Similar TGA-TPO studies to those performed in the present work were also conducted [43], where 20.7 wt% "carbon" was measured after 5 h on reaction stream as opposed to the present 5 wt% Ni/CeO_2 catalyst, where an amount of 19.6–37.7 wt% C was found but after a much longer duration (25 h) on reaction stream (W_{cat}/F = 0.001–0.002 g min/cm^3); no W_{cat}/F data were reported in Ref. [43]. The mild deactivation observed in the 8 wt% Ni/CeO_2 catalyst [43] was proposed to be the result of strong metal-support interactions occurred after hydrogen reduction at 700 °C, where Ni particles were covered by a thin layer of ceria reduced support. The latter was evidenced by HRTEM and the inability for hydrogen chemisorption [43].

The high stability of the present 5 wt% Ni/CeO_2 catalyst is in harmony with the practically unchanged particle size of Ni in the fresh and spent catalysts as determined by XRD and the fact that catalyst's reduction in H_2 at 700 °C caused no suppression in hydrogen chemisorption. TEM-EDX analysis and mapping of several catalyst samples was performed on nickel grains (e.g. Fig. S6 for the 5 wt% $Ni/Ce_{0.2}Pr_{0.8}O_2$ catalyst). Over none of the imaged nickel grains EDX responses at characteristic positions of the l shell transitions (Ce at 4.83 and 5.26 keV, Pr at 5.02 and 5.49 keV) or m shell transitions (Ce at 883 eV and Pr at 929 eV) could be confirmed. As a result, no

covering or decoration of Ni grains with Ce or Pr occurred over the catalysts tested.

A very interesting work concerning changes in morphology induced by strong metal-support interactions on Ni/CeO_2 during H_2 reduction and DRM at 750 °C was reported by Gonzalez-DelaCruz et al. [44]. The authors have used *in situ* XAS analysis where under dry reforming the Ni *K*-edge X-ray absorption spectrum parameters obtained (after fitting analysis) suggested changes in the size and morphology of nickel particles. In particular, the authors suggested that reduced ceria surface allowed the formation of new Ni particles spreading on the partially reduced ceria support, which could account for a lower value in the mean Ni coordination number, resulting in some kind of strong metal-support interactions responsible for catalyst's stability at 750 °C. This morphological change, however, was not stable after cooling of the sample in H_2 flow to room T.

The stability of Ni-based catalysts in dry reforming with deposition of significant amounts of "carbon" in the form of filaments, as in the present case (Fig. 6), depends on the position of the Ni particles [43,45]. The latter may either stay at the top of the filament or may be enclosed within the filament leading to a loss of active nickel surface, thus to catalyst deactivation. In the present 5 wt% Ni/CeO_2 catalyst Ni crystallites at the tip of the carbon nanotubes were seen after 25 h of DRM according to HRTEM images (Fig. S11), which show detachment of the metal particles from the CeO_2 support. It should be noted that filamentous carbon formation was significantly influenced by the Ni particle size and occurred mostly over Ni particles larger than 7 nm for the Ni-alumina aerogel catalysts [46].

On the basis of the above offered discussion, the present 5 wt% Ni/CeO_2 catalyst, synthesized, calcined and reduced according to the procedures mentioned in Section 2.1, appears very competitive compared to other ceria-supported Ni catalysts evaluated for dry reforming at 750 °C. The large amount of "coke" deposited is the only severe problem faced by this catalytic system for practical applications, where tuning of the Pr-dopant loading in the ceria matrix can provide an excellent catalytic system highly resistant to coking for dry reforming (at least in the 700–750 °C range) as discussed below.

4.1.2. $Ni/Ce_{1-x}Pr_xO_{2-\delta}$

Only very recently [10] Pr-doped CeO_2 (in the presence of Hf-dopant) was investigated as support of nickel (10 wt% Ni) for the development of a durable and active DRM catalyst in the 600–900 °C range. The doped-ceria support was synthesised using the EDTA-citrate method, whereas Ni was deposited via the solvothermal method. The fresh $Ni/Ce_{0.65}Hf_{0.25}Pr_{0.1}O_{2-\delta}$ catalyst was calcined at 450 °C and reduced in hydrogen at 700 °C for 2 h before reaction. A nickel mean particle size of 10–15 nm was reported [10]. The catalyst was tested at 800 °C using a feed composition of $CH_4:CO_2 = 2:1$ and a GHSV of 23,000 h^{-1}, where an extremely stable catalytic performance after 150 h on stream was reported in terms of CH_4-conversion (~55%), CO_2-conversion (~96%) and H_2/CO ratio (~0.75). Characterisation of the spent catalyst by HRTEM revealed no "carbon" formation after 150 h on reaction stream. On the other hand, $Ni/Ce_{0.65}Hf_{0.35}O_{2-\delta}$ exhibited reduced catalytic activity and H_2-selectivity and a large decrease in X_{CH4}, X_{CO2} and H_2/CO performance parameters.

The above described catalytic performance of Pr-doped CeO_2-HfO_2 supported Ni appears different to the one obtained in the present work (5 wt% Ni supported on Pr-doped CeO_2). In particular, the progressive introduction of Pr into the ceria lattice resulted in the progressive reduction in all catalytic performance parameters (X_{CH4}, X_{CO2}, H_2/CO) as illustrated in Fig. 3 and Fig. S8 (Supplementary Information), as opposed to the Pr-doped CeO_2-HfO_2 catalyst [10]. On the other hand, the long-term stability of the Ni/CeO_2 in DRM at 750 °C was only slightly reduced when Pr was introduced into the ceria lattice (Fig. 4), result which is similar to the one obtained with the Pr-doped CeO_2-HfO_2 supported Ni [10].

4.1.3. Understanding the $Ni/Ce_{1-x}Pr_xO_{2-\delta}$ DRM catalytic performance

In order to understand the catalytic performance of the present $Ni/Ce_{1-x}Pr_xO_{2-\delta}$ solids (Figs. 3 and 4) the initial reaction rate (Fig. 10) and the SSITKA (Figs. 8 and 9 and Table 4) results obtained become important. According to the reaction rate results (Fig. 10), the rates of hydrogen formation over Ni/CeO_2, $Ni/Ce_{0.8}Pr_{0.2}O_{2-\delta}$ and $Ni/Ce_{0.2}Pr_{0.8}O_{2-\delta}$ catalysts after 2 h on reaction stream at 550 °C were found to be 6.4, 6.3 and 4.0 μmol H_2 g^{-1} s^{-1}, respectively. Considering the fact that the H_2/CO ratio over these catalysts was found to be 0.60, 0.69 and 0.65, respectively, then the CO formation rates are 10.7, 9.1 and 6.2 μmol CO g^{-1} s^{-1}, respectively. On the basis of the TOF_{ITK} (s) and the concentration of *active* "carbon" reaction intermediates, N_C, which are estimated independently by SSITKA (Table 4), the rate of CO formation via the CO_2 activation route ($R_{CO/CO2}$, μmol g^{-1} s^{-1}) can be estimated via Eq. (9). For the Ni/CeO_2, $Ni/Ce_{0.8}Pr_{0.2}O_{2-\delta}$ and $Ni/Ce_{0.2}Pr_{0.8}O_{2-\delta}$ catalysts, this rate was found to be 6.30, 6.55, and 4.35, μmol g^{-1} s^{-1}, respectively (Table 4). Based on the X_{CH4} (%) (Table 4), the rate of CO formation via the CH_4 activation route ($R_{CO/CH4}$, μmol g^{-1} s^{-1}) can also be estimated (via a material balance) and this is found to be 3.07, 2.87 and 1.4 μmol CO g^{-1} s^{-1}, respectively, for Ni/CeO_2, $Ni/Ce_{0.8}Pr_{0.2}O_{2-\delta}$ and $Ni/Ce_{0.2}Pr_{0.8}O_{2-\delta}$ catalysts. Considering the fact that the kinetic rate of CO formation under steady-state reaction conditions ($R_{CO,tot}$, Fig. 10) must be the sum of the rate of CO formation via the CO_2 activation route (measured by SSITKA) and that via the CH_4 activation route (measured independently from SSITKA), one should remark that the carbon material balance is within 4–12%.

The SSITKA analysis revealed that the *site reactivity* (TOF_{ITK}, s^{-1}), a unique parameter estimated only by the SSITKA technique, follows the order TOF_{ITK} ($Ce_{0.8}Pr_{0.2}O_{2-\delta}$) > TOF_{ITK} ($Ce_{0.2}Pr_{0.8}O_{2-\delta}$) > TOF_{ITK} (CeO_2), whereas the activity order (R_{rxn} per mass of catalyst) is as follows: R_{rxn} (CeO_2) ≅ R_{rxn} ($Ce_{0.8}Pr_{0.2}O_{2-\delta}$) > R_{rxn} ($Ce_{0.2}Pr_{0.8}O_{2-\delta}$). This important result strongly suggests that tuning of the DRM activity of 5 wt% $Ni/Ce_{0.8}Pr_{0.2}O_{2-\delta}$ could be performed by an increase in the number density of *active sites* (sites g_{cat}^{-1}) which possess *larger site reactivity* (TOF_{ITK}, s^{-1}) than that of Ni/CeO_2 and $Ni/Ce_{0.2}Pr_{0.8}O_{2-\delta}$ catalytic systems. The nature of these *active* catalytic sites is discussed below.

Regarding the extent of "carbon" deposition, the effect of Pr present in the crystal lattice of ceria support is remarkable. According to the results of Table 2 and Figs. 5 and 6, after 25 h of DRM at 750 °C and using a W_{cat}/F of 10^{-3} g min/cm^3, the amount of "carbon" accumulated on the $Ni/Ce_{0.8}Pr_{0.2}O_{2-\delta}$, $Ni/Ce_{0.5}Pr_{0.5}O_{2-\delta}$ and $Ni/Ce_{0.2}Pr_{0.8}O_{2-\delta}$ catalysts, respectively, drops by a factor of ~90, 245 and 280 with respect to Ni/CeO_2; an amount of only 70 mg C g_{cat}^{-1} was found for the latter catalyst. When W_{cat}/F was doubled, or equivalently the GHSV was decreased to half, the $Ni/Ce_{0.2}Pr_{0.8}O_{2-\delta}$ also caused reduction by a factor of ~250 in the amount of "carbon" compared to the Ni/CeO_2 catalyst. On the basis of these results, it is clear that reduction in the activity and H_2/CO product-gas ratio observed over the $Ni/Ce_{1-x}Pr_xO_{2-\delta}$ (x = 0.2–0.8) catalysts compared to Ni/CeO_2 (see Figs. 3 and 4 and Table 2) cannot be ascribed to the deposition of an increased amount of *inactive* "carbon". In particular, as Pr-dopant concentration increases from 0 to 20 atom-% the "carbon" formation rate is largely decreased and is accompanied only by a small decease in CH_4 and CO_2 conversions and H_2/CO ratio. However, further progressive increase of Pr-dopant concentration to 80 atom-% leads to a significant drop in

all three catalytic performance parameters and to a lesser extent in "carbon" deposition.

We have previously reported [25] (use of other than SSITKA transient isotopic experiments) on the main elementary reaction steps of the DRM over the present 5 wt% Ni/$Ce_{0.8}Pr_{0.2}O_{2-\delta}$ catalytic system. The presence of oxygen vacant sites in the $Ce_{1-x}Pr_xO_{2-\delta}$ support was suggested as a potential *active* site for the dissociation of CO_2 to CO(g) and re-oxidation of the reduced support surface (CO_2 activation route):

$$CO_2(g) + \square\text{-s(support)} \rightarrow CO(g) + \text{O-s(support lattice oxygen)}. \quad (10)$$

On the other hand, Hartwig et al. [47] in a recent elegant work have investigated the temperature-dependent oxygen vacancy formation, oxygen release and lattice rearrangement of $Ce_{1-x}Pr_xO_{2-\delta}$ (x = 0.2–0.6) thin films. They reported that after increasing the Pr-dopant loading a decreasing O_2 desorption temperature and an increasing CO_2 desorption temperature were observed. Furthermore, O_2-TPD and XRD results agreed in that by increasing Pr-dopant loading OSC and lattice spacing increase; the latter has also been verified in the present work for a wider Pr-dopant concentration range; x = 0.2–0.8 (see Table S1 and Fig. S1). The O_2-TPD and CO_2-TPD investigations of Hartwig et al. [47] can be offered to explain the significant reduction in the rate of "carbon" accumulation on Ni/$Ce_{1-x}Pr_xO_{2-\delta}$ (x = 0.2–0.8) due to an increased oxygen mobility in the $Ce_{1-x}Pr_xO_{2-\delta}$ matrix which favours "carbon" oxidation to CO(g). This important elementary reaction step is found in the CO_2 activation path and it is recognized for some time now as the main contributor to the control of the rate of "carbon" accumulation in CeO_2-doped supported Ni catalysts [10,16,48–52]. What was not reported so far is the participation of the oxygen vacancies in the $Ce_{1-x}Pr_xO_{2-\delta}$ solids not only in the dissociation of CO_2 (Eq. (10)) but also in the formation of adsorbed "carbonate-type" species reversibly interacting with gaseous CO_2 under dry reforming conditions in the 550–750 °C range (Scheme 1). This type of "carbonate" is considered as *inactive* species, which could block active sites of the CO_2 activation path. The CO_2 stored reversibly on the catalyst surface (N_{CO2}, Table 4) could justify the drop in activity of the Ni/$Ce_{1-x}Pr_xO_{2-\delta}$ (x = 0.2–0.8) catalysts. At 750 °C, where the latter effect is significant (see Figs. 4, S8 and 10 b), the amount of this "CO_2-pool" shown in Scheme 1 is increased by a factor of 1.58 and 2.1, respectively, when Ni/CeO_2 is compared to Ni/$Ce_{0.8}Pr_{0.2}O_{2-\delta}$ and Ni/$Ce_{0.2}Pr_{0.8}O_{2-\delta}$ catalysts. At the same time, the H_2 formation rate is decreased by a factor of ~1.1 and 2.2, respectively. A similar comparison can be also made at 550 °C, where the size of the "CO_2-pool" increases by a factor of 1.52 and the H_2 formation rate decreases by a factor of 2.2 when Ni/CeO_2 is compared to Ni/$Ce_{0.2}Pr_{0.8}O_{2-\delta}$. The fact that the size of the "CO_2-pool" after 2 h of DRM may depend on the concentration of gas phase CO_2, then strict comparison should be made at similar X_{CO2} conversions; see DRM at 550 °C (Table 4).

In a recent work [22] the role of multivalent Pr in the formation and migration of oxygen vacancy in $Ce_{1-x}Pr_xO_{2-\delta}$ (x = 0.0–0.5) solids was investigated. The following conclusions are important and relevant to the results of the present work. First, Pr^{3+} and Pr^{4+} are incorporated as majority and minority ions, respectively, where Pr^{3+} play a key role in the generation of oxygen vacancies during the replacement of Ce^{4+} with Pr^{3+}. Second, addition of Pr^{3+} causes a local distortion near the oxygen vacancy due to the mismatch between Pr^{3+} and Ce^{4+} and the bond length between each species with oxygen. Third, the atomic level role of the electronic states of the incorporated elements (Ce^{4+}/Ce^{3+} and Pr^{3+}/Pr^{4+}) can tune the oxygen mobility and the concentration and stability of oxygen vacant sites. In another investigation of the $Ce_{1-x}Pr_xO_{2-\delta}$ (x = 0, 0.1, 0.5 and 0.9) solids [37], it was demonstrated that the stated Ce-Pr-O solid compositions consisted of a single fluorite solid solution phase without the formation of additional Ce- or Pr-based oxides (secondary phases). XPS results revealed a rather good agreement between nominal (bulk) and surface stoichiometries, and only a slight tendency toward segregation of the lower concentration cation (Pr in $Ce_{0.9}Pr_{0.1}O_{2-\delta}$ and Ce in $Ce_{0.1}Pr_{0.9}O_{2-\delta}$) from the bulk to the surface. When these materials were tested for CH_4 oxidation, maximum catalytic activity was observed for the $Ce_{0.5}Pr_{0.5}O_{2-\delta}$ solid.

The above offered discussion on the $Ce_{1-x}Pr_xO_{2-\delta}$ solid solution used as support of 5 wt% Ni in the present work tends to suggest that the opposite trend in the rate of "carbon" deposition and that of DRM (CO_2 activation path) might be partially due to the influence of Pr-doping on the strength of associative CO_2 chemisorption and on its dissociative counterpart onto the oxygen vacant sites present adjacent to anionic oxygen and metal cationic (Ce^{3+}, Ce^{4+}, Pr^{3+} and Pr^{4+}) sites. This could result in the adjustment of available *active* oxygen vacant sites and likely adjacent ones for CO_2 dissociation (Eq. (10)).

The catalytic performance and the amount of inactive "carbon" formed towards the RWGS (20%CO_2/7%H_2/He; GHSV = 30,000 h^{-1}) at 750 °C were evaluated over the 5 wt% Ni/$Ce_{0.8}Pr_{0.2}O_{2-\delta}$ solid [25]. It was found that the X_{CO2} (%) for the RWGS was 22% for the Ni/$Ce_{0.8}Pr_{0.2}O_{2-\delta}$, where the X_{CO2}(%) to CH_4 was less than 0.1%. The amount of inactive "carbon" formed after 1 h of RWGS was found to be significantly lower (~0.7 mg/g_{cat}) than that formed after 1 h of DRM. Also, the X_{CO}(%) of methanation reaction (2.5%CO/7.5%H_2/He) at 750 °C was less than 2% after 1 h of DRM [25]. On the basis of these results, since the most active Ni/$Ce_{0.8}Pr_{0.2}O_{2-\delta}$ in the series of Ni/$Ce_{1-x}Pr_xO_{2-\delta}$ (x = 0.2–0.8) solids exhibits a larger H_2/CO ratio than the catalysts with larger Pr-dopant loadings (Fig. 3, 750 °C), it is clear that differences in the RWGS behaviour alone cannot explain the different activity and product selectivity for these catalytic systems. The fact that the H_2/CO ratio in most of the experimental conditions used is lower than one, and the X_{CO2}(%) is larger than that of X_{CH4}(%) (Fig. 3 and Table S2), the RWGS reaction does proceed to some extent in all catalytic systems, in general agreement with literature reports [2,10–19].

4.2. SSITKA – kinetic and mechanistic studies

The SSITKA results presented in Figs. 8 and 9 and Table 4 should be appreciated in relation with the discussion offered in the previous Section 4.1.3. A SSITKA analysis of the dry reforming of CH_4 at high temperatures (e.g. 750 °C) was attempted for the first time over ceria-based supported Ni, aiming at an accurate quantification of important kinetic parameters, such as the surface concentration ($\mu mol\, g^{-1}$ or θ) of *active* "carbon-containing" reaction intermediates formed in the CO_2 activation path leading to the formation of CO, the life-time of such intermediates (τ_C, s) and the TOF_{ITK} (s^{-1}). Furthermore, the presence of a pool of *inactive* adsorbed CO_2 which reversibly interacts with the catalyst surface was identified. The nature of the *active "carbon"* pool "C"-s shown in Scheme 1 can be discussed on the basis of the N_C quantity (Table 4) and the TEM-EDXS results (Section 3.5.2). In the case of Ni/CeO_2, DRM at 750 °C for 2 h resulted in an equivalent amount of θ_C = 3.4 (based on the Ni surface). The fact that the CO-s pool appeared in Scheme 1 must be considered very small ($\theta_{CO\text{-}s} << 1$), it can be concluded that the nature of *active* "carbon" cannot be in the atomic state on the Ni surface but either as small 3-D clusters or thin films of likely few atomic layers on the surface of Ni particles. The latter is evidenced by the HRTEM images shown in Fig. S7a,b (Supplementary Information). The carbon in the thin films deposited on selected areas of the Ni surface may not all be regarded as *active* carbon. Another possible explanation for the nature of active "carbon" and its concentra-

tion level exceeding one Ni_s monolayer (Ni/CeO_2) could arise from the work of Verykios and his co-workers [29,53,54] over Ni/La_2O_3. SSITKA work provided evidence that $La_2O_2CO_3$ *active* species were formed during dry reforming leading to CO(g) via several decomposition pathways by the assistance of adsorbed H-s and C-s species on Ni and/or Ni-lanthana interface [29]. We do not exclude the presence of such oxy-carbonate species on the present $Ni/Ce_{1-x}Pr_xO_{2-\delta}$ catalysts, a subject of future investigation. Sokolov et al. [55] have reported initial TOF_{CH4} rates as a function of Ni particle size for the Ni/La_2O_3-ZrO_2 catalytic system. It was shown that higher TOF rates were obtained on the larger Ni particles, result that was related to the presence of $La_2O_2CO_3$ at the Ni-support interface, which react slowly (RDS) with C-s formed on Ni (via CH_4 decomposition), leading to CO(g) and restoration of support's CO_2 chemisorption sites.

Bobin et al. [48] investigated supported Ni on similar carriers as in the present work ($Ln_x(Ce_{0.5}Zr_{0.5})_{1-x}O_2$; Ln = Pr, Sm) in one of the few SSITKA works reported for DRM over supported Ni catalysts. One of the important results found was that the reaction rate of surface carbonates towards CH_4 was significantly lower than that of CH_4 or CO_2 dissociation. This result could be related to the present findings that a pool of carbonate-type adsorbed species reversibly interacting with gaseous CO_2 should be considered as spectator(s). Other important conclusions from the same SSITKA work [48] (4%CO_2, $CH_4/CO_2 = 1$) similar to the one used in the present work, are as follows: (a) CH_4 activation proceeds independently of CO_2 activation; (b) CO_2 does not interact with $-CH_x$ derived from CH_4 decomposition (no transfer of ^{13}C derived from $^{13}CO_2$ into $^{12}CH_4$); (c) fast rate of CO_2 dissociation on support sites and high surface oxygen mobility providing fast oxygen transfer from support sites to Ni sites (CH_4 activation); (d) negligible surface coverage of active "carbon"; (e) irreversible CH_4 interaction and reversible CO_2 interaction with the catalyst surface; (f) rate of catalyst re-oxidation by CO_2 largely exceeds that of its reduction by CH_4; (g) reactive oxygen species of support at the Ni-support interface are apparently bound with pairs of Ce^{4+} and Pr^{3+}. The "carbon" and SSITKA measurements of the present work (Tables 2 and 4) and other transient isotopic work performed on the 5 wt% $Ni/Ce_{0.8}Pr_{0.2}O_{2-\delta}$ catalyst [25] support the above conclusions (a), (c), (e) and (g).

The dependence of TOF_{ITK} (s^{-1}) on support chemical composition that provides the true site reactivity for each supported Ni surface can be utilised to tailor the activity of DRM on this specific catalytic system. Detailed information acquired from HRTEM investigations on the surface structure of Ni particles could lead to a desired correlation between TOF_{ITK} (s^{-1}) and Ni structure (e.g. density of exposed facets). It is rather clear that the TOF_{ITK} (s^{-1}) behaviour on the present supported Ni catalysts cannot be correlated with the Ni particle size but rather with the specific Ni surface structure (e.g. ratio of different crystallographic faces) for similar in size Ni particles. This important issue is a subject of future investigation.

Sadykov et al. [49] have reported on important mechanistic issues of dry reforming on Pt/Ce-Zr-Pr-O via mathematical modelling of the non isotopic transient response curves of H_2, CO, CO_2 and CH_4, similar to those of H_2 formation rate depicted in Fig. 10. It was shown that the character and shape of response curves is mainly defined by the rates of carbonates formation and consumption, the rate of oxygen diffusion from the support surface/subsurface to the Pt-support interface and the interaction of CO_2 with vacant sites on the Pt surface. In analogy to their findings and those of this work, a first attempt to explain the transient features of the H_2 formation rate at 550 °C in the first 2 min (Fig. 10a) is as follows. Due to the likely higher oxygen mobility in $Ce_{0.2}Pr_{0.8}O_{2-\delta}$ than $Ce_{0.8}Pr_{0.2}O_{2-\delta}$ or CeO_2 support, the rate of "carbon" oxidation to CO(g) and "carbon" deposition by CH_4 decomposition appears faster. This feature leads to no overshoot in the rate of H_2 formation. As the reforming temperature increases to 750 °C, slight differences are only observed in the shape of the initial H_2 formation rates (Fig. 10b), suggesting that surface coverages for important reaction intermediates and vacant sites may change only to a small extent.

5. Conclusions

The following conclusions can be derived from the results of the present work:

(i) 5 wt% Ni supported on $Ce_{1-x}Pr_xO_{2-\delta}$ carrier was found to be a very promising "coke" resistant active catalytic material towards dry reforming of methane in the 700–750 °C range. The increase in the concentration of *inactive* chemisorbed CO_2 on support sites with increasing Pr-dopant loading in the ceria matrix was found to correlate with the activity drop.

(ii) The catalytic activity order on a mass basis over the investigated series of 5 wt% $Ni/Ce_{1-x}Pr_xO_{2-\delta}$ solids of similar Ni particle size and dispersion does not correlate with the activity order in terms of TOF_{ITK} (s^{-1}). In particular, 5 wt% Ni/CeO_2 with the largest catalytic activity ($\mu mol\ H_2\ g^{-1}\ s^{-1}$) exhibits about five times lower TOF_{ITK} (s^{-1}) at 550 °C than 5 wt% $Ni/Ce_{0.8}Pr_{0.2}O_{2-\delta}$ which has a similar activity per gram basis. This result is related to the larger θ_C/τ_C ratio associated with the TOF of the catalytic cycle measured at reaction conditions.

(iii) The concentration of *active* "carbon" formed under dry reforming strongly depends on the Pr-dopant concentration in the ceria matrix and the reaction temperature. The former is crucial since it regulates the mobility and concentration of lattice support oxygen near the Ni-support interface, thus leading eventually to gaseous CO. Also, Pr-dopant regulates the concentration of surface support oxygen vacancies, largely responsible for the dissociation of CO_2 to form CO(g) and atomic O (re-oxidation of the reduced support).

(iv) Introduction of Pr-dopant into the ceria support matrix at the level of 20 atom-% drastically reduces the rate of "carbon" deposition compared to the Ni/CeO_2, while keeping high activity and product selectivities similar to those obtained by Ni/CeO_2.

(v) Inactive carbon in filamentous and graphitic structure is largely formed in the Ni/CeO_2 catalyst after 25 h of dry reforming at 750 °C (20% CH_4; $CH_4/CO_2 = 1$) as deduced by SEM and XRD. Islands of carbon in several areas on the Ni particle's surface were also identified by HAADF/STEM.

Acknowledgements

The Research Committee of the University of Cyprus is gratefully acknowledged for financial support of this work.

Appendix A. Supplementary data

Supplementary data associated with this article can be found, in the online version, at http://dx.doi.org/10.1016/j.apcatb.2016.03.012.

References

[1] M. Usman, W.M.A. Wan Daud, H.F. Abbas, Renew. Sustain. Energy Rev. 45 (2015) 710–744.
[2] D. Pakhare, J.J. Spivey, Chem. Soc. Rev. 43 (2014) 7813–7837.
[3] A.W. Budiman, S.-H. Song, T.-S. Chang, C.-H. Shin, M.-J. Choi, Catal. Surv. Asia 16 (2012) 183–197.
[4] D. Li, Y. Nakagawa, K. Tomishige, Appl. Catal. A: Gen. 408 (2011) 1–24.
[5] M.-S. Fan, A.Z. Abdullah, S. Bhatia, ChemCatChem 1 (2009) 192–208.
[6] Y.H. Hu, E. Ruckenstein, Adv. Catal. 48 (2004) 297–345.
[7] X.E. Verykios, Chem. Ind. 56 (6) (2002) 238–255.
[8] J.R.H. Ross, Catal. Today 100 (2005) 151–158.

[9] J.A. Farmer, C.T. Campbell, Science 329 (2010) 933–936.
[10] D. Harshini, D.-H. Lee, Y. Kim, S.-W. Nam, J.-H. Han, H.-C. Ham, C.-W. Yoon, Catal. Lett. 144 (2014) 656–662.
[11] H. Eltejaei, H.R. Bozorgzadeh, J. Towfighi, M.R. Omidkhah, M. Rezaei, R. Zanganeh, A. Zamaniyan, A.Z. Ghalam, Int. J. Hydrogen Energy 37 (2012) 4107–4118.
[12] T. Sukonket, A. Khan, B. Saha, H. Ibrahim, S. Tantayanon, P. Kumar, R. Idem, Energy Fuels 25 (2011) 864–877.
[13] A. Kambolis, H. Matralis, A. Trovarelli, Ch. Papadopoulou, Appl. Catal. A: Gen. 377 (2010) 16–26.
[14] J. Chen, Q. Wu, J. Zhang, J. Zhang, Fuel 87 (2008) 2901–2907.
[15] P. Kumar, Y. Sun, R.O. Idem, Energy Fuels 22 (2008) 3575–3582.
[16] P. Kumar, Y. Sun, R.O. Idem, Energy Fuels 21 (2007) 3113–3123.
[17] H.-S. Roh, H.S. Potdar, K.-W. Jun, J.-W. Kim, Y.-S. Oh, Appl. Catal. A: Gen. 276 (2004) 231–239.
[18] J.A. Montoya, E. Romero-Pascual, C. Gimon, P. Del Angel, A. Monzón, Catal. Today 63 (2000) 71–85.
[19] S. Wang, G.Q. Lu, Appl. Catal. B: Environ. 19 (1998) 267–277.
[20] M.S. Aw, M. Zorko, P. Djinović, A. Pintar, Appl. Catal. B: Environ. 164 (2015) 100–112.
[21] M.S. Aw, I.G.O. Črnivec, P. Djinović, A. Pintar, Int. J. Hydrogen Energy 39 (2014) 12636–12647.
[22] K. Ahn, D.-S. Yoo, D.H. Prasad, H.-W. Lee, Y.-C. Chung, J.-H. Lee, Chem. Mater. 24 (2012) 4261–4267.
[23] Z. Song, W. Liu, H. Nishiguchi, A. Takami, K. Nagaoka, Y. Takita, Appl. Catal. A: Gen. 329 (2007) 86–92.
[24] P. Shuk, M. Greenblatt, Solid State Ionics 116 (1999) 217–223.
[25] M.M. Makri, M.A. Vasiliades, K.C. Petallidou, A.M. Efstathiou, Catal. Today 259 (2015) 150–164.
[26] F. Wang, L. Xu, J. Zhang, Y. Zhao, H. Li, H.-X. Li, K. Wu, G.-Q. Xu, W. Chen, Appl. Catal. B: Environ. 180 (2016) 511–520.
[27] H.M. Swaan, V.C.H. Kroll, G.A. Martin, C. Mirodatos, Catal. Today 21 (1994) 571–578.
[28] M.A. Goula, A.A. Lemonidou, A.M. Efstathiou, J. Catal. 161 (1996) 626–640.
[29] V.A. Tsipouriari, X.E. Verykios, J. Catal. 187 (1999) 85–94.
[30] K.C. Petallidou, S. Boghosian, A.M. Efstathiou, Catal. Today 242 (2015) 153–167.
[31] K.C. Petallidou, K. Polychronopoulou, S. Boghosian, S. García-Rodríguez, A.M. Efstathiou, J. Phys. Chem. C 117 (2013) 25467–25477.
[32] K.C. Petallidou, A.M. Efstathiou, Appl. Catal. B: Environ. 140–141 (2013) 333–347.
[33] B. Li, S. Zhang, Int. J. Hydrogen Energy 38 (2013) 14250–14260.
[34] K. Polychronopoulou, C.N. Costa, A.M. Efstathiou, Appl. Catal. A: Gen. 272 (2004) 37–52.
[35] A.M. Efstathiou, X.E. Verykios, Appl. Catal. A: Gen. 151 (1997) 109–166.
[36] A.M. Efstathiou, J.T. Gleaves, G.S. Yablonsky, in: M. Che, J.C. Vedrine (Eds.), Characterization of Solid Materials: From Structure to Surface Reactivity, vol. 2, Wiley-VCH Weinheim, Germany, 2012, pp. 1013–1073 (Chapter 22).
[37] S. Somacescu, V. Parvulescu, J.M. Calderon-Moreno, S.-H. Suh, P. Osiceanu, B.-L. Su, J. Nanopart. Res. 14 (2012) 885–901.
[38] R. Razzaq, C. Li, N. Amin, S. Zhang, K. Suzuki, Energy Fuels 27 (2013) 6955–6961.
[39] F. Ocampo, B. Louis, L. Kiwi-Minsker, A.-C. Roger, Appl. Catal. A: Gen. 392 (2011) 36–44.
[40] K. Asami, X. Li, K. Fujimoto, Y. Koyama, A. Sakurama, N. Kometani, Y. Yonezawa, Catal. Today 84 (2003) 27–31.
[41] S. Wang, G.Q. Lu, Energy Fuels 12 (1998) 248–256.
[42] S.S. Kim, S.M. Lee, J.M. Won, H.J. Yang, S.C. Hong, Chem. Eng. J. 280 (2015) 433–440.
[43] H. Ay, D. Üner, Appl. Catal. B: Environ. 179 (2015) 128–138.
[44] V.M. Gonzalez-Delacruz, J.P. Holgado, R. Pereñíguez, A. Caballero, J. Catal. 257 (2008) 307–314.
[45] D. San-José Alanso, J. Juan-Juan, M.J. Illán-Gómez, M.C. Román-Martínez, Appl. Catal. A: Gen. 371 (2009) 54–59.
[46] J.-H. Kim, D.J. Suh, T.-J. Park, K.-L. Kim, Appl. Catal. A: Gen. 197 (2000) 191–200.
[47] M. Hartwig Zoellner, G. Niu, J.-H. Jhang, A. Schaefer, P. Zaumseil, M. Bäumer, T. Schroeder, J. Phys. Chem. C 117 (2013) 24851–24857.
[48] A.S. Bobin, V.A. Sadykov, V.A. Rogov, N.V. Mezentseva, G.M. Alikina, E.M. Sadovskaya, T.S. Glazneva, N.N. Sazonova, M.-Y. Smirnova, S.A. Veniaminov, C. Mirodatos, V. Galvita, G.B. Marin, Top. Catal. 56 (2013) 958–968.
[49] V.A. Sadykov, E.L. Gubanova, N.N. Sazonova, S.A. Pokrovskaya, N.A. Chumakova, N.V. Mezentseva, A.S. Bobin, R.V. Gulyaev, A.V. Ishchenko, T.A. Krieger, C. Mirodatos, Catal. Today 171 (2011) 140–149.
[50] T.-J. Huang, H.-J. Lin, T.-C. Yu, Catal. Lett. 105 (2005) 239–247.
[51] F.B. Noronha, E.C. Fendley, R.R. Soares, W.E. Alvarez, D.E. Resasco, Chem. Eng. J. 82 (2001) 21–31.
[52] P. Djinović, I.G.O. Črnivec, B. Erjavec, A. Pintar, Appl. Catal. B 125 (2012) 259–270.
[53] X.E. Verykios, Int. J. Hydrogen Energy 28 (2003) 1045–1063.
[54] Z. Zhang, X.E. Verykios, Appl. Catal. A: Gen. 138 (1996) 109–133.
[55] S. Sokolov, E.V. Kondratenko, M.-M. Pohl, U. Rodemerck, Int. J. Hydrogen Energy 38 (2013) 16121–16132.